Revision submitted to *Géotechnique*, September 2019 -

Equivalent state theory for sand with non-plastic fine mixtures: A DEM investigation

by

N. Barnett[1], M.M. Rahman[2], M.R. Karim[3], H.B.K. Nguyen[4] and J.A.H. Carraro[5]

1. Nick Barnett
   PhD Candidate, Natural and Built Environments Research Centre
   School of Natural and Built Environments
   University of South Australia, Mawson Lakes, SA 5095, Australia
   Tel: +61 (0)8 830 23740
   Email: Nick.Barnett@unisa.edu.au
2. Md. Mizanur Rahman, M ASCE
   Associate Professor in Geotechnical Engineering
   Water and Natural Resources Strand Leader, Natural and Built Environments Research Centre
   School of Natural and Built Environments
   University of South Australia, Mawson Lakes, SA 5095, Australia
   Tel: +61 (0)8 830 25899, Fax: +61 (0)8 830 25082
   Email: Mizanur.Rahman@unisa.edu.au
3. Md. Rajibul Karim
   Lecturer, School of Natural and Built Environments
   University of South Australia, Mawson Lakes, SA 5095, Australia
   Email: Rajibul.Karim@unisa.edu.au
4. H.B.K Nguyen
   Research Associate, School of Natural and Built Environments
   University of South Australia, Mawson Lakes, SA 5095, Australia
   Email: Khoi.Nguyen@unisa.edu.au
5. J.A.H. Carraro
   Senior Lecturer in Experimental Geotechnical Engineering
   Department of Civil and Environmental Engineering
   Imperial College London, UK
   Email: antonio.carraro@imperial.ac.uk

Words in the Text: 7227

Table: 3

Figures: 19

ABSTRACT:

DEM was used to simulate constant volume (undrained) triaxial compression tests for coarse particles (sand) mixed with non-plastic fines. The fines content (f_c) of the mixtures tested was kept equal to 0, 0.05, 0.10 or 0.20. Accordingly, the critical state and micromechanical responses of these mixtures were evaluated. A focus on the influence of f_c on sand behaviour was captured when $f_c < f_{thre}$, where f_{thre} represents a threshold fines content, which corresponds to a transition between a fines-in-sand soil matrix to a sand-in-fines soil matrix. DEM was utilised to assess the micromechanical participation of fine particles within the sand skeleton (matrix). Such evaluations led to assessing the performance of the equivalent granular void ratio (e^*), the equivalent granular state parameter (ψ^*), and ultimately their inherent parameter *b*, which represents the proportion of fines actively participating in the sand skeleton structure. It was observed that through capturing the stress partition of contact types within granular mixtures, a reasonable approximation of the active proportion of contacts within the sand matrix could be obtained leading to a DEM interpretation of the *b* parameter. The study therefore evaluated the concept and applicability of the equivalent state theory for sand-fines mixtures.

Key words: Discrete element method, undrained behaviour, critical state theory, equivalent state theory.

1 INTRODUCTION

The critical state (CS) data points obtained from a series of triaxial tests conducted on specimens of a sandy soil is mathematically defined by dp'=dq=dΔu=dε_v=0. Such data points form a unique critical state line (CSL) in p'-q and e-log p' spaces; where p', q, Δu, ε_v and e denote the mean effective normal stress, deviatoric stress, pore water pressure change, volumetric strain, and void ratio, respectively. The CSL in e-log p' space is the anchoring concept of Critical State Soil Mechanics (CSSM) framework, as it may be used as a reference line to predict soil behaviour. Soil with a state (i.e. e and p') above the CSL exhibits contractive behaviour, whilst states below the CSL exhibit dilative behaviour. Been and Jefferies (1985) presented, the state parameter (ψ), to quantify such relative location by the difference between the current e and the e on the CSL at the same p'. Accordingly, a condition of ψ>0, corresponds to contractive behaviour whilst ψ<0 corresponds to dilative behaviour. Many researchers found correlations between ψ and characteristic features of soil behaviour such as instability behaviour (Huang et al. 2014; Nguyen et al. 2017; Perez et al. 2016; Yang 2002), excess pore water pressure (Qadimi and Coop 2007; Zhang et al. 2018), phase transformation and characteristic states (Murthy et al. 2007; Nguyen et al. 2018), and cyclic shear behaviour (Qadimi and Coop 2007). Subsequently, ψ has been encapsulated within state-dependent constitutive models (Jefferies 1993; Manzari and Dafalias 1997).

The CSSM framework has been validated and is well understood for clean sands and clays. However, many granular soils are mixtures of sands and fines (particle sizes smaller than 0.063 or 0.075mm, according to (BS 5930) or (ASTM D2487-17), respectively), where sands may contain varying amounts of non-plastic fines (Cubrinovski et al. 2010; Rahman and Sitharam 2019). The application of CSSM framework for sand mixed with non-plastic fines is challenging as the CSL moves downwards in e-log p' space with the increase in fines content, f_c (i.e. mass of fines over the total mass of soil solids) up to a threshold fines content, f_{thre} which represents a fines content, corresponding to a transition between a fines-in-sand soil matrix to a sand-in-fines soil matrix (Thevanayagam et al. 2002). The influence of f_c may still be evaluated under CSSM framework, provided that the CSL and the corresponding ψ specific to the f_c under consideration is used. Thus, although it may be necessary to obtain the CSLs for each f_c, it is a laborious task which offers significant practical and theoretical challenges (Rahman et al. 2014). Therefore, attempts have been made that consider the clean sand behaviour as a reference and then capture the effect of f_c by- (1) developing empirical relations (e.g. multiplying factors) for each f_c relative to the behaviour of the host sand (Kenney 1977); (2) correcting e to an equivalent void ratio (e^*) on the assumption that only a fraction of fines participate to the force skeleton structure of sand-fines mixtures (Rahman et al. 2008; Thevanayagam et al. 2002); (3) evaluating the performance of ψ for different granular mixtures (Yang et al. 2018). While approach 1 and 3 require predefined CS data and CSLs, respectively, to define reduction factors and ψ, the e^* in approach 2 requires an estimation of a fraction of active f_c via b parameter (discussed later), which may be obtained using empirical/semi-empirical equation/s of soil grading properties (Mohammadi and Qadimi 2015; Ni et al. 2004; Rahman et al. 2008), making the approach independent of predefined soil test data/CSLs. CSLs for sand with f_c<f_{thre}, may coalesce to a single equivalent granular critical state line (EG-CSL) in e^*-log p' space. The EG-CSL unifies many CSSM frameworks for sand-fines mixtures to a single CSSM framework, given that f_c<f_{thre}. Similarly to the definition of ψ, an equivalent granular state parameter (ψ^*) can be obtained by replacing e with e^* yielding a unique CSL in the EG-CSL framework (Rahman and Lo 2007). Importantly, it has been shown that ψ^* also correlates with characteristic features of sand-fines mixtures such as the undrained instability stress ratio, η_{IS} (Rahman and Lo 2012), phase transformation and other characteristic states of cyclic shear behaviour (Baki et al. 2014; Rahman et al. 2014). Further, by use of ψ^*, equivalent state dependent constitutive models which predict the behaviour of sand-fines mixtures have been developed (Lashkari 2014; Rahman et al. 2014). The use of e^* within CSSM will be referred to as equivalent state theory (EST), hereafter. Although EST has been used for correlating key characteristics of soil behaviour with ψ^* and developing a single constitutive model for $f_c < f_{thre}$, as CSSM has been used for sands/clays, a criticism is that the micromechanical interpretation of non-active/active f_c in force skeleton structure is hypothetical and its physical basis is not well understood (Carrera et al. 2011; Yang et al. 2015). Therefore, a brief evolution of EST and corresponding assumptions that needed micromechanical evaluation are presented below.

It is worth mentioning that the early conceptual development of e^* came from efforts on determining the non-active clay content in granular phase structure (Mitchell 1976). Shen et al. (1977), Kenney (1977) and Troncoso and Verdugo (1985) who used natural sand-fines mixtures and tailings, respectively, reported no fines participated in the skeleton structure, i.e. granular material strength remained the same with addition of fines, but their e reduces. Following Mitchell (1976), Kuerbis et al. (1988) treated fines as voids to obtain the skeleton void ratio, e_{sk}, i.e. e_{sk} represents the force skeleton structure of the sand matrix which does not require the b parameter. Later, Kuerbis et al. (1988) and others found consistent characteristic behaviour with e_{sk} for sand-fines mixtures at low f_c (Chu and Leong 2002; Georgiannou et al. 1990). Although a different expression of e_{sk} was proposed by these researchers, e_{sk} can be simply written as $e_{sk} = (e + f_c)/(1 - f_c)$ when fine and coarse particles share an identical specific gravity. However, it was reported that the quality of correlations between characteristic behaviour with e_{sk} were reduced for higher f_c (Zlatovic and Ishihara 1995). Pitman et al. (1994) presented scanning electron microscope (SEM) imagery showing that some portion of fines comes in between sand particles at f_c=0.20. The assumption that all fines are non-active (i.e., void) in e_{sk} calculations was therefore shown to be incorrect at least for higher f_c. Therefore, the fraction of f_c that contributes to the force structure was considered, and e^* was proposed (Thevanayagam et al. 2002):

$$e^* = \frac{e + (1-b)f_c}{1-(1-b)f_c} \tag{1}$$

where b represents the fraction of f_c that contribute to the force structure. As mentioned earlier, there are two micromechanical assumptions in Eq. 1 for e^*– (1) with the addition of f_c, there is a fraction of non-contributing f_c in force skeleton structure (for the same e) which reduces the characteristic strengths; (2) a fraction of f_c contributes to force skeleton structure at higher f_c and b may represent the fraction of f_c that contributes to the force skeleton structure i.e. to deviatoric stress, q. These assumptions are often challenged, criticised and require further evaluation.

Evaluating these assumptions i.e. active/non-active f_c and quantifying b throughout the duration of loading via experimental means (e.g. SEM, CT scan) may be particularly challenging, expensive and may not be generally applicable for all sand-fines mixtures. However, discrete element method (DEM) has the capability of generating a numerical assembly of particles with a desired grain size distribution whilst allowing an in-depth understanding of the micromechanics of individual particles or an entire assembly, which is suitable to evaluate the above assumption. Although many DEM studies evaluated the CS behaviour of clean sand (Huang et al. 2014; Kuhn 2016; Nguyen et al. 2017; Nguyen et al. 2018; Yan and Dong 2011; Zhao and Guo 2013), very few studies have evaluated the CS behaviour of sand-fine mixtures (Ng et al. 2016; Zhou et al. 2018). One of the reasons for such few studies may be due to huge computational demand required when fines are modelled in DEM. However, there are few studies reporting simulations with sand-fines mixtures (Ng et al. 2016; Yin et al. 2014; Zhou et al. 2018; Zhou et al. 2016). Using DEM, Zhou et al. (2018) showed that there is a downwards shift of the CSL in e-log p' space, for f_c<f_{thre}, which is consistent with earlier experimental research showing the same trend (Murthy et al. 2007;

Zlatovic and Ishihara 1995). Studying binary mixtures of ellipsoids, Ng et al. (2016) observed *e* at CS as a function of f_c. However, both CS studies of sand-fines mixtures were not studied under an equivalent state framework, and therefore the concept of e^* within CSSM framework has not been evaluated. Although not operating within CSSM framework, using 2D DEM, Dai et al. (2015) analysed the influence of f_c in the sand matrix and whilst suggesting findings may relate to e^* and particularly *b*, a clear linkage between the two was not attempted and therefore there were no clear advances to EST. Shire et al. (2016) evaluated the influence of a stress reduction factor, α (Skempton and Brogan 1994) on the original definition of e^* (i.e. where *b* is ignored) and observations suggested that the stress participation of fines could be related to the activity/inactivity of fines. However, there was no clear scope to provide physical basis to a *b* parameter. Through 1D compression simulations in DEM, Minh and Cheng (2014) suggested a unique normal compression line (NCL) could be achieved using e^*, if *b* is considered to be the ratio between the volume of "involved" fine particles to the total volume of fine particles. However, their study did not evaluate CS behaviour. In fact, many DEM studies which examine sand-fines behaviour, have done so using many different variations of *e* (Ng et al. 2016; Rahman et al. 2017; Yin et al. 2014; Zhou et al. 2018), which further highlights the degree of uncertainty in best quantifying the density index for sand-fines mixtures.

Therefore, DEM is used to simulate undrained triaxial compression tests whereby the effect of non-plastic fines on the behaviour of granular material, their characteristic features and CS response are all evaluated. The assumption of EST is also evaluated, allowing for the physical basis of *b* to be further examined. The micromechanical perspective of DEM allows for particulate aspects of soil behaviour such as contact density, soil fabric and contribution to force skeleton to be evaluated. Fundamental behaviour sand with non-plastic fines is further characterised and explained through such an approach.

2 DISCRETE ELEMENT METHOD (DEM)

DEM employs a force-displacement law in conjunction with Newton's second law to capture the motion and interactions between neighbouring particles at small time increments (Cundall and Strack 1979). Inter-particle contact forces are computed using a contact model which exhibits the overall mechanical behaviour of a granular assembly. In this study, a rolling resistance linear contact model (RRLCM) was deployed for inclusion of the rolling resistance mechanism (Fig. 1) to the conventional linear contact model. Therefore, a rolling resistance coefficient (μ_r), in addition to an inter-particle friction coefficient (μ), was installed at each contact. Following Gong and Liu (2017), μ_r=0.3 was adopted for both sand and fines. The Young's modulus (E) and Poisson's ratio (ν) which describe deformability of particles were represented in the contact model by the effective modulus (E^*), and ratio between normal and tangential contact stiffness (k^*). The normal stiffness (k_n), tangential stiffness (k_s) and rolling stiffness (k_r) were a function of E^* and k^* as presented below.

$$k_n = \frac{AE^*}{L}\ ; k_s = \frac{k_n}{k^*}\ ; k_r = k_s \bar{R}^2 \qquad (2)$$

where A is equivalent contact area, L is length of contact, and $\bar{R}$ is the effective radius between contacting pieces (Iwashita and Oda 1998). Equation (2) ensured that the contact stiffness were particle size dependent via A and L (Yan and Dong 2011). A summary of input parameters is presented in Table 1.

2.1 Sample preparation technique

The DEM software, PFC^{3D}, was used to undertake conventional, isotropically compressed constant volume (undrained) triaxial simulations for clean sand (f_c=0) and sand mixed with non-plastic fines (f_c=0.05, 0.10 and 0.20). Fig. 2a-d illustrate the various assemblies of sand-fines mixtures used in this study. The particle size distribution (PSD) of coarse material was identical to Sydney sand (Rahman et al. 2014), and is referred hereafter as sand. The coefficient of uniformity (C_u=D_{60}/D_{10}) and the median particle size (D_{50}) of sand are 1.26 and 0.279mm respectively. Non-plastic fine particles were monodisperse spheres with a diameter (d) of 0.035mm, and are referred hereafter as fines. Fines were selected on two considerations- 1) to reduce the required number of particles in the assembly, i.e. reduce computational expenses and, 2) to form a "fines-in-sand" matrix where the effective diameter ratio of sand and fines (χ=D_{10}/d) is large enough so that fines may be trapped or moveable within the densest possible packing of sand particle. Simple geometric calculation suggests that χ should be ≥ 6.5 to satisfy the above conditions (Lade et al. 1998). Following many researchers, D_{10} was considered as the representative sand size (Ni et al. 2004; Rahman and Lo 2008). Therefore, χ=6.5 (=0.230/0.035) was maintained in this study. The particle size distribution curves for sand and fines used in this study are shown in Fig. 3. The range of void ratio after consolidation (e_0) for specimens with each f_c as per Fig. 4 illustrates the wide range of densities that were considered in simulation. Fig. 4 suggests that e_{max} and e_{min} were reduced with the addition of fines, given that f_c<f_{thre}. The trend is qualitatively consistent with the e_{max} and e_{min} of clean Sydney sand (Bobei et al. 2009) and Cambria sand-fine mixtures (Lade et al. 1998) which can be explained by fines increasingly occupying void spaces with the rise in f_c (Cubrinovski and Ishihara 2002; Lade et al. 1998). The Cambria sand-fine mixture also consisted of rounded sand particles and non-plastic fines, and therefore the similar qualitative relationship illustrated in Fig. 4 is encouraging for DEM simulations.

DEM samples were prepared via a staged isotropic compression, where particles were initially generated within a box defined by six frictionless-rigid walls and then gradually compressed until a small isotropic stress (equal to approximately one-tenth of the isotropic consolidation stress (Ng et al. 2016)) was developed on each of the walls. Throughout this process, a μ value (termed μ_{sp}) between 0 and 1 was assigned to achieve a desired density; a large μ_{sp}

achieved a loose assembly whilst a small μ_{sp} achieved a dense assembly. Then, μ was reset to 0.50 and the triaxial simulation commenced. Isotropic compression was achieved via a servo-control mechanism applied to each wall, which ensured a constant and isotropic boundary stress, whilst volume-changing compression occurred. Constant volume (CV) shearing was achieved via strain control of the top and bottom walls (i.e. acting as loading platens), whilst remaining walls were controlled respectively to ensure no volumetric change. A summary of the simulations is shown in Table 2.

2.2 Numerical stability of simulations

Rigid boundaries may inflict uncharacteristically large friction angles in small assemblies and therefore the accuracy and consistency of the results may depend on the specimen size (Huang et al. 2014; Zhao and Guo 2013; Zhou et al. 2017). The specimen size (or number of particles, N) should be large enough to minimize the influence of the end-restraint conditions. Therefore, two sand specimens with f_c=0.10, T307 and T310, were prepared at similar initial states of p'_0=94kPa and e_0=0.547±0.002, but different N of 129266 and 144506, respectively, to evaluate the influence of N. Here, subscript "0" corresponds to the post-consolidation reading. The influence of N on CV behaviour in q-ε_q and q-p' spaces was negligible (given the large discrepancy in computational demand) as presented in Fig. 5. This suggested a representative volume can be achieved with N of 129266 for sand with f_c=0.10. A slight discrepancy in Fig. 5, may be explained by the difference in e_0. Note, achieving a desirable e_0 in DEM simulations is challenging (Nguyen et al. 2017).

In DEM the chosen shear strain rate should achieve static equilibrium (Sitharam et al. 2009), near quasi-static condition (Nguyen et al. 2017) and consistent CS behaviour (Andrade et al. 2012). Thus, the influence of strain rate was also assessed for sand with f_c=0.10 in Fig. 5. T307 had a strain rate of ε=0.001s^{-1}, which was 2.5 times smaller than that used in T308 (ε=0.0004s^{-1}). The negligible discrepancy in their behaviour in q-ε_q and q-p' spaces, intuitively, suggested that ε

of 0.001s^{-1} was suitable to achieve numerical stability of sand with f_c=0.10. Identical processes were used to find suitable N and ε for other granular mixtures.

The unbalanced force ratio (UFR), which is defined as the ratio of average unbalanced forces acting over all bodies to the average contact force acting over all bodies, provides a measurement of the state of equilibrium within the system. A state of quasi-static equilibrium has been deemed to be achieved when UFR<10^{-2} (Ng 2006). Conservatively, in this study, quasi-static conditions were assumed when UFR<10^{-4}.

3 RESULTS OF CONSTANT VOLUME TRIAXIAL SIMULATION

The major and minor principal stresses were computed based on the stress tensor equation as suggested by Christoffersen et al. (1981):

$$\sigma_{ij}^{'} = \frac{1}{V} \sum_{c \epsilon N_c} f_i^c \, l_j^c \tag{3}$$

here, $\sigma_{ij}^{'}$ is the effective stress tensor, V is the assembly volume, N_c is the total number of contacts, f_i^c is the i^{th} component contact force at contact c and l_j^c is the j^{th} branch vector connecting the centres of two contacting particles at contact c. Some DEM studies computed stress quantities considering the contact forces acting upon the rigid boundaries (Gu et al. 2014). However, the stress tensor which considers only internal contact forces was utilised in this study to reduce the likelihood of rigid boundaries expressing artificial behaviour (Fu and Dafalias 2011; Marketos and Bolton 2010).

3.1 Influence of e on CV behaviour of sand-fines mixtures

The influence of e_0 on the CV behaviour of sand with f_c=0.10 was observed for three samples prepared at p'_0=94kPa (Fig. 6). Three different behaviours were observed depending on e_0. T307 with e_0 of 0.545 exhibited non-flow (NF) behaviour i.e. strain hardening occurred until the CS in

q-ε_q and q-p' spaces (Fig. 6a-b) and thus can be classified as dense sand. T312 had the largest e_0 of 0.746 and exhibited flow (F) liquefaction behaviour i.e. an initial small strain hardening to a peak deviatoric stress (q_{peak}) and then strain softened until reaching a low CS stress. This behaviour is also known as static liquefaction. T309 with e_0 of 0.711 can be classified as intermediately dense and exhibited limited flow (LF) behaviour, i.e. after initial strain hardening to a q_{peak}, it exhibited mild strain softening (almost unnoticeable in this case) followed by phase transformation and subsequent strain hardening towards CS. For both T309 and T312, strain softening, i.e. $\mathrm{d}q/\mathrm{d}\varepsilon_q < 0$ is a form of undrained instability which is triggered at the onset of flow liquefaction (Murthy et al. 2007), and quantified by the instability stress ratio $\eta_{IS}=(q/p')_{peak}$ (Fig. 6b). η_{IS} can be used to explain the triggering of static/cyclic liquefaction (Baki et al. 2012; Rahman et al. 2014). For both NF and LF i.e. T307 and T309, the effective stress paths (ESP) in q-p' space initially moved leftward signifying initial contractive tendencies and then moved rightward (showing dilative tendencies). The change from contractive to dilative tendencies can be identified by $\mathrm{d}\Delta u_e=0$ in Δu_e-ε_q space as shown in Fig. 6c (Sukumaran et al. 1996). This change is coined by the term phase transformation (PT) state. In the constant volume (CV) simulation, the real Δu that would develop in a truly undrained test was approximated to be the difference in p' between drained and constant volume loading paths (Sitharam et al. 2008). The manuscript refers to this quantity as the equivalent change in pore water pressure, $\Delta u_e=p'_D-p'_{CV}$ where subscripts "D" and "CV" denote drained and constant volume loading paths. The stress ratio at PT (η_{PT}) is another characteristic feature used in bounding surface model to capture the evolution from contractive to dilative behaviour (Manzari and Dafalias 1997). The micromechanics for both η_{IS} and η_{PT} have been studied for granular materials (sands) in DEM (Huang et al. 2014; Rahman et al. 2018) and added significant value for fabric dependent constitutive modelling (Gao et al. 2014). However, the observed η_{IS} and η_{PT} for sand-fines mixtures in this study via DEM is new and its micromechanics is further discussed within CSSM framework in later section.

T307 failed to reach a condition of Δu_e=0 and therefore strictly did not reach a CS. In this case, an extrapolation method was used to obtain the CS (Carrera et al. 2011; Nguyen et al. 2017; Rahman and Lo 2014). When called upon, the changing rate of equivalent pore water pressure, $\delta(\Delta u_e)/\delta\varepsilon_q$ was plotted with stress ratio, η. The value of $\eta_{CS}=M$ was estimated through extrapolating $\delta(\Delta u_e)/\delta\varepsilon_q$ to 0 (i.e. CS). Then, p' at CS was estimated in η-p' space by extrapolating η to M, as discussed in Rahman and Lo (2014). In this study, most of the simulations reached CS at the end of CV shearing, however few simulations failed to reach clear CSs, warranting the extrapolation technique.

3.2 *Influence of f_c on CV behaviour of sand-fines mixtures at similar e_0*

Fig. 7 presents the CV responses of three samples (T10, T311 and RT321) with similar e_0 and p'_0 but with varying f_c of 0, 0.05 and 0.10 in q-ε_q, q-p', Δu_e-ε_q and CN-ε_q spaces. All samples exhibited NF behaviour, however a significant reduction in strain hardening was observed with increasing f_c (Fig. 7a). This is in line with the common experimental supposition that fines-in-sand soil matrixes form a meta-stable fabric where some f_c is active in the sand skeleton, causing higher compressibility and lower q and p' (Yamamuro and Lade 1998). Another interesting observation was even though q and p' decreased with f_c, the slope of CSL (M) in q-p' space is not affected significantly (Fig. 7b). This is further investigated in subsequent sections. The increase in compressibility with f_c was also supported by the generation of Δu_e with f_c (Fig. 7c).

The coordination number (CN=2C/N) proposed by Rothenburg and Bathurst (1989) is a micromechanical entity which measures the contact density of granular assemblies; where C represents the total number of contacts and N represents the total number of particles.

Alternatively, Thornton (2000) proposed a mechanical coordination number (Z_m=(2C-N_1)/(N-N_0-N_1)); where N_1 and N_0 denote the number of particles which contain one and zero contacts, respectively. Particles which contain less than one contact are considered mechanically inactive and thus, Z_m provides a measure of mechanical contacts (contacts contributing to the stable state of stress) per particle. Fig. 7d shows the evolution of CN and Z_m with shearing. Despite shearing commencing at similar initial states (i.e. similar e_0, p'_0) for T10, RT321 & T311, the CN values significantly decreased with the addition of f_c, suggesting a large fraction of f_c floated within the sand matrix and did not contribute to force skeleton structure. Ng et al. (2016) also reported a large amount of fines to be floating within the void of granular mixtures for similar fine contents.

For clean sand (T10), the observed Z_m path followed a similar trend to the CN path, although Z_m was slightly larger in magnitude. Nguyen et al. (2018) reported similar findings in the case of drained behaviour of clean sand. For sand-fine mixtures (RT321 & T311), the Z_m path is considerably higher than their CN counterparts. This may be explained by the large number of fines introduced to the mixtures which contain less than one contact, in turn giving rise to Z_m. In agreement, the DEM study of Dai et al. (2015), found fine particles to be less active within the force skeleton structure as they are easily confined within void spaces.

3.3 Influence of f_c on contact force network

The contact force network, which represents the direction of contact forces and their magnitudes at CS, are presented in Fig. 8 for the three simulations previously shown in Fig. 7. The diagrams show all contact forces within the assembly at CS, and each contact is represented by a coloured column, where the contacts colour and thickness provide a measure of the contact force magnitude. The strong force contacts, defined by the contact forces which are closely aligned with the axis of compression i.e. $\sigma_{axial}>\sigma_{radial}$ (Radjai et al. 1998), promote enhanced interlocking and shear resistance capabilities at CS. Alternatively, strong contacts may be quantified as a contact which inherits a force larger than the average force (Radjai et al. 1998) experienced in the assembly, at any given stage during shearing. Based on this definition, the proportion of particles in strong force contacts was considerably larger for clean sand than sand-fines mixtures. Table 3 depicts the proportion of fine and sand particles involved in strong contacts at CS for the three mixtures. For example, the proportion of fines active in an assembly was calculated as the number of fines particles with contact forces larger than the average contact force at CS over the total amount of fines. For T10, 39% of particles were involved in a strong contact at CS. For both RT321 and T311, only 5% of all particles were involved in a strong contact at CS. For the same two mixtures, 92% and 93% of sand particles were involved in a strong contact, respectively, highlighting that a large fraction of fines did not contribute to force skeleton structure. Hence, a large concentration of the deviatoric stress component is via involvement of sand particles. Both these findings and those in Fig. 7 support the assumption of EST that only a fraction of fines participate to the force skeleton structure of sand-fines mixtures.

3.4 Contribution of fines to deviatoric stress, q

The contribution of fines to the force skeleton structure, e.g. deviatoric stress, can be evaluated by decomposing the stress tensor into three additive variants respective of their contact type as follows:

$$\sigma'_{ij} = \sigma'^{S-S}_{ij} + \sigma'^{S-F}_{ij} + \sigma'^{F-F}_{ij} \tag{4}$$

where σ'^{S-S}_{ij}, σ'^{S-F}_{ij} and σ'^{F-F}_{ij} denote the stress tensor computed based only on the sand-to-sand, sand-to-fines and fines-to-fines contacts, respectively. Therefore, contact types and their corresponding contribution to the deviatoric stress can be identified to assess their contribution to force skeleton structure. Fig. 9a and Fig. 9b illustrate the contribution of each contact type to the deviatoric stress in q-ε_q space, for specimens T303 and T307 which had f_c of 0.05 and 0.10, respectively. T303 and T307 had similar initial states of (e_0=0.567, p'_0=94kPa) and (e_0=0.545,

p'_0=94kPa) respectively. Despite the slight discrepancy of e_0 (increased density), the reduction of strength with increasing f_c was observed again. Evidently, sand-to-sand contacts made up nearly all of the deviatoric stress for both specimens and therefore, the deviatoric stress generated from fines-to-fines contacts ($q_{f\text{-}f}$) and sand-to-fines contacts ($q_{s\text{-}f}$) was small. For T303 and T307, sand-to-sand contacts were responsible for 97.8% and 94.9% of the total deviatoric stress at CS, respectively. The slight reduction of sand-to-sand participation can be explained by the increase in f_c. Fine particles provided little structural value to the sand matrix and were rarely involved in force skeleton structure (less than 6% contribution to CS deviatoric stress in both instances). However, it is worth noting that the deviation between q and $q_{s\text{-}s}$ is due to the partition of $q_{s\text{-}f}$ with increasing f_c, suggesting a fraction of f_c were involved in the force skeleton structure. Although RT315 (Fig. 9c) had a lower e_0 of 0.428 for f_c=0.20, it exhibited a similar trend i.e. additional fines increased participation to q, although behaviour of the sand matrix was largely dominated by sand-to-sand contacts. 87% of the total CS deviatoric stress for RT315 was generated via sand-to-sand contacts, thus fines approximately contributed to 13% of the deviatoric stress at CS.

The ESPs for each contact type for T303 (with f_c=0.05) and RT315 (with f_c=0.20) are presented in Fig. 10a and Fig. 10b respectively. The $q_{s\text{-}f}$, $q_{f\text{-}f}$, $p'_{s\text{-}f}$ and $p'_{f\text{-}f}$ at the beginning of CV shearing for T303 were almost zero, however, $q_{s\text{-}f}$ and $p'_{s\text{-}f}$ evolved to small finite values at CS (29kPa and 21kPa, respectively) whilst $q_{f\text{-}f}$ and $p'_{f\text{-}f}$ remained infinitesimal. This suggests that some sand-to-fines contacts contributed to force skeleton structure for f_c=0.05. However, fines-to-fines contact contribution was negligible. Again, the $q_{s\text{-}f}$, $p'_{s\text{-}f}$, $q_{f\text{-}f}$, and $p'_{f\text{-}f}$ at the beginning of CV shearing for RT315 were almost zero, however, at CS they evolved to values of 120kPa, 117kPa, 11kPa and 34kPa, respectively. Thus, sand-to-fines contacts manifested larger contribution than fines-to-fines contacts. Comparing T303 to RT315 suggests that the contribution of fines to the force skeleton structure via sand-to-fines contacts increased with increasing f_c. As the contribution of fines-to-fines contacts is negligible, the contribution of fines to the force structure may be approximated by sand-to-fines contacts.

The *CN* was also decomposed into components based on each contact type:

$$CN_{s-s} = \frac{2C_{s-s}}{N_s}\ ;\ CN_{s-f} = \frac{2C_{s-f}}{N}\ ;\ CN_{f-f} = \frac{2C_{f-f}}{N_f} \tag{5}$$

where N_s and N_f denote the number of sand and fine particles, respectively. $C_{s\text{-}s}$, $C_{s\text{-}f}$ and $C_{f\text{-}f}$ represent the average amount of sand-to-sand, sand-to-fines and fines-to-fines contacts per particle, respectively. The CN-ε_q and Z_m-ε_q paths for different contact types for T303 and T307 are presented in Fig 11a and Fig. 11b, respectively. Interestingly, T303 (inheriting a larger dilative tendency than T307 as per Fig. 9) yielded a lower *CN* (*CN*=0.57 at CS) than T307 (*CN*=0.92 at CS). Therefore, the classical *CN* does not provide an accurate contact density index to reflect the dilative tendencies of sand-fines mixtures. However, *CN*s-s seemingly better reflects the macroscopic dilative tendencies. Two conclusions to be drawn from these observations are: 1) a proportion of fine particles are likely to be involved in contact which may provide small structural value, and 2) sand-to-sand contacts largely govern dilative tendencies of sand-fines mixtures, when $f_c \leq 0.20$. Interestingly, the Z_m and $CN_{s\text{-}s}$ paths closely approximate each other for both sand-fine mixtures. The observation supports both above conclusions. That is, sand-to-sand contacts form a large majority of the mechanical contacts formulated in each granular mixture (i.e. $Z_m \approx CN_{s\text{-}s}$), whilst sand-to-fine contacts are likely to form the residual mechanical contacts.

3.5 Critical State Behaviour of sand-fines mixtures

The CS data points for all simulations are presented in *q*-*p'* space as shown in Fig. 12. The slope of the CSL (i.e. *M*) changed slightly for each mixture, within the range $1.09 \leq M \leq 1.25$. Although the relationship of *M* with f_c was relatively random. When the clean sand *M*-line (*M*=1.15) was assumed over $0 \leq f_c \leq 0.20$, an R^2=0.995 was obtained. Rahman et al. (2014) presented a unified state-dependent constitutive modelling framework for sand-fine mixtures over a range of f_c, through the assumption that M was independent of f_c. The observations per Fig. 12 suggest such an assumption to somewhat reflect realistic behaviour of sand-fine mixtures.

Alike the assumption, some experimental observations regarding sand mixed with low-plasticity fines have observed M may be independent of f_c (Bouckovalas et al. 2003; Huang et al. 2004; Rahman et al. 2014; Rahman et al. 2011; Zlatovic and Ishihara 1995). Although unspecified in majority of these studies, the work of Rahman et al. (2014) used a fine mixture which contained round and smooth fines (Majura silt) (Rahman 2009). On the other hand, studies have observed that M increases with f_c (Carraro et al. 2009; Murthy et al. 2007; Ni et al. 2004; Papadopoulou and Tika 2008). From these studies, Carraro et al. (2009) and Murthy et al. (2007) specified the shape of fine particles to be very angular, which potentially caused an increased in M as f_c increased. The behavior of M with f_c could therefore be a relationship which is influenced by fine shape, relative to sand shape.

The CS data points for each granular mixture are plotted in the e-log p' space as shown in Fig. 13a. These CS points yielded non-linear CSLs for sand with each f_c, which shifted downwards with increasing f_c. These CSLs can be represented by the following power function (Li et al. 1999):

$$e_{cs} = e_{lim} - \lambda({p'}_{cs}/p_a)^{\xi} \tag{6}$$

where λ of 0.027 and ξ of 0.90 for all f_c suggesting CSL parallelism. e_{lim} values were 0.875, 0.820, 0.750 and 0.630 for f_c of 0, 0.05, 0.10 and 0.20, respectively. The findings coincide with experimental observations (Rahman and Lo 2014; Rahman et al. 2011; Thevanayagam et al. 1997).

To evaluate the EST, the e in Fig. 13a was converted to e^* using equation (1). The b parameter was estimated using the semi-empirical equation presented in the appendix (Eq. A1). The values of b were 0.08, 0.15 and 0.30 for f_c of 0.05, 0.10 and 0.20, respectively. This approach has been used in many other studies (Baki et al. 2014; Rahman and Lo 2012; Rahman and Lo 2014) and has been evaluated with new emerging datasets by independent researchers with general acceptability being observed for poorly graded sand and fines mixture (Lashkari 2014; Mohammadi and Qadimi 2015). Alternatively, the b parameter can be estimated by the contribution of contact types to q, as explored in subsequent sections. In e^*-log p' space (Fig. 13b) all CS data points coalesce with the original CSL of clean sand. Note, e=e^* for clean sand, therefore the EG-CSL is same as the CSL for clean sand. Therefore, the e^* may unify four CS datasets for sand with four f_c to a single equivalent state framework. It was observed that CS data points for $p'_{cs} > 100kPa$ coalesce well on the EG-CSL. However, despite minor scatter for $p'_{cs} < 100kPa$, the EG-CSL has a coefficient of determination, R^2=0.969.

When the CS data points are plotted in e_{sk}-log p' space a family of CSLs form, i.e. no EG-CSL, with a higher deviation for a higher f_c, is observed (Fig. 13c). For low f_c (i.e. f_c=0.05) CS data points relatively align with those of clean sand and a CSL irrespective of f_c within this range could be assumed. Although, as f_c increases and fines become active in the force skeleton the CS data points deviate from the clean sand CSL (e.g. f_c=0.20). The definition of e_{sk} may be valid for low f_c, although as observed in Fig. 8-10, the role of fines in the skeleton structure increases at larger f_c. Therefore, e_{sk} which neglects the mechanical role of fines may not be an applicable density index, especially at the larger end of f_c<f_{thre}. Along with this limitation of e_{sk}, obtaining ψ_{sk} for each granular mixture is challenging as no unified CSL irrespective of f_c is developed. Thus, ψ^* is used in subsequent sections as a state index for granular mixtures.

3.6 DEM interpretation of b parameter

The active fine particles that contribute to the sand-skeleton structure, i.e. the original definition of b, could be captured in DEM through evaluating the contribution of fine particles to q i.e. $q_{f\text{-}f}$

and $q_{s\text{-}f}$ with respect to the contribution of sands to q i.e. $q_{s\text{-}s}$. Thus, a DEM version of the b parameter can be approximated as:

$$b' = \frac{q_{sf(cs)} + q_{ff(cs)}}{q_{ss(cs)}}\ ; \quad \text{where } 0 < b' < 1 \tag{10}$$

where b' denotes an alternative measure of b parameter. Eq. 10 satisfies the mathematical requirement of b i.e. b'=0 when $q_{sf(cs)} + q_{ff(cs)} = 0$ for f_c=0, b'=1 when $q_{sf(cs)} + q_{ff(cs)} = q_{ss(cs)}$ for f_c=1.0 and is only valid for when f_c<f_{thre}. However, the b' obtained in this approach was not constant for χ and f_c, but they varied with e and p' i.e. each simulation had a slightly different b'. Therefore, the range of b' values were 0.02 to 0.05, 0.05 to 0.16 and 0.13 to 0.37 for f_c of 0.05, 0.10 and 0.20, respectively. The semi-empirical value of b, as discussed earlier, was slightly higher than b' for f_c of 0.05, however both b and b' were comparable for higher f_c of 0.10 and 0.20. To evaluate EST with b', b' was substituted for b in Eq. 1 and a DEM-versioned e^* (e^*_{DEM}) was developed. In Fig. 14, e^*_{DEM} of each test is projected with the existing EG-CSL (by semi-empirical approach). e^*_{DEM} data points are shown to skew slightly from e^* data points (compare with Fig. 13b). Overall, the e^*_{DEM} and e^* data points showed similar agreement with the EG-CSL. Specifically, an R^2=0.969 was yielded when e^* was projected with the EG-CSL (Fig. 13b) and when e^*_{DEM} was used instead, an R^2=0.953 results (Fig. 14). The experimental Sydney sand data was also added in Fig. 14. There is slight difference between CSLs by DEM and experiment. However, the trend of the data, particularly the curvature of the CSL, is similar. Although these DEM simulations, with a RRLCM and monodisperse fines, did not intend to match Sydney sand data, the observed behavioural trend were similar.

3.7 Micromechanics at CS for sand-fines mixtures

Previous studies reported that *CN* at CS also forms a unique relation in *CN*-log p' space (Gu et al. 2014; Nguyen et al. 2017). However, for sand with f_c, *CN*-p' relations were non-unique (Fig. 15a).

For f_c=0.05, the CN-p' relation shifted downward, further indicating that a large fraction of f_c floated in the void spaces of the matrix. However, the CN-p' relation shifted upwards slowly with increasing f_c ($0.05 \leq f_c \leq 0.20$), indicating a gradual increase of the fraction of f_c that are contact-involved. This is analogous to the active fraction of f_c for higher f_c. Therefore, the CN for sand-to-sand and sand-to-fines (CN_{ss+sf}) as a measure of skeleton structural contact density are presented in CN_{ss+sf}-p' space as shown in Fig. 15b. A single correlation with R^2= 0.976 was obtained. In Z_m-p' space (R^2=0.810) (Fig. 15c) a similar trend followed, thus $Z_m \approx CN_{ss+sf}$. Although, CN_{ss+sf} slightly better reflected the stress state at CS for the entire family of granular mixtures. Herein, CN_{ss+sf} will be the contact density index used as it seemingly best reflects the macro-mechanical behaviour of all granular mixtures.

3.8 ψ and ψ for sand-fines mixtures and their characteristic behaviour*

The CSL for each f_c in Fig. 13a and corresponding e_0 and p'_0 for each test can be used to define the post-consolidation state parameter, ψ_0. In this case, four CSSM datasets have to be developed for four different f_c to evaluate relations between characteristic behaviour i.e. PT state, and the undrained instability state with ψ. Alternatively, the EG-CSL in conjunction with e^*_0 and p'_0 can be used to define ψ^*_0. The advantage of ψ^*_0 is that it only requires EG-CSL which is mathematically equivalent to CSL for clean sand or can be derived from a CSL for a f_c , but may applicable for other f_c (when f_c<f_{thre}) (Rahman and Lo 2008). In this case, four CSSM datasets are unified into a single EST dataset, which has to be evaluated for the relations between characteristic behaviour and ψ^*_0. Note, the numerical value of ψ and ψ^* are not equal but very close, and their relation can be presented via the following function:

$$\frac{\psi}{\psi *} = 1 - (1 - b) f_c \quad (7)$$

3.8.1 Relation between PT with ψ and ψ for sand-fines mixtures*

The PT state can be approximated as the point where dilatancy (d) becomes zero. Setting d=0 in the dilatancy equation of the SANISAND constitutive model as detailed in Li and Dafalias (2000): $d = 0 = \mathrm{d}\varepsilon_v^p/\mathrm{d}\varepsilon_q^p = d_0/M[Mexp(m\psi) - \eta]$, one can achieve $\eta_{PT}=(q/p')_{PT}=M \exp(-m\psi)$. The η_{PT} and ψ_0 data points in Fig. 16a shows a good R^2 (=0.880), which can be approximated by a similar exponential function as embedded in the SANISAND model. To evaluate the EST, the ψ^*_0 was plotted with η_{PT} in Fig. 16b. In η_{PT}-ψ^*_0 space an R^2=0.867 is yielded when the data is represented by the same function as in Fig. 16a. Similar correlations were therefore observed for both ψ_0 and ψ^*_0 with η_{PT} within the range of $0 \leq f_c \leq 0.20$.

To further evaluate the sand-fines interaction, the CN_{ss+sf} at η_{PT} ($CN_{ss+sf(PT)}$) as a measure of skeleton structural contacts are presented in $CN_{ss+sf(PT)}$-ψ_0 space as shown in Fig. 16c. Although some scatter, the relation exhibits explainable behaviour i.e. a dilative sample has negative ψ_0 and therefore at η_{PT} a higher CN_{ss+sf} was achieved. In $CN_{ss+sf(PT)}$-ψ^*_0 space (Fig. 16d), the trend is very much similar to what is observed in Fig 16c, further suggesting the appropriateness of ψ^*_0 as a state index for sand-fines mixtures.

Yoshimine and Ishihara (1998) proposed an entity called the flow potential, $u_F = 1 - p'_{PT}/p'_0$ which characterises the generation of Δu at PT. The relationship between u_F and ψ_0, and u_F and ψ^*_0 are depicted in Fig. 17a and Fig. 17b, respectively. Despite some scatter, u_F showed a single trend with ψ^*_0, irrespective of f_c. This finding also highlights the encouraging performance of ψ^*_0 in predicting characteristic features. Similar performance of ψ_0 and ψ^*_0, was again observed for the studied f_c range.

3.8.2 Relation between η_{IS} and ψ^* for sand-fines mixtures

Many researchers suggested that η_{IS} exhibits good correlation with ψ (Rabbi et al. 2019; Yang 2002) and has also been implemented in constitutive models (Imam et al. 2002). Rahman and Lo (2012) presented very good correlations in η_{IS}-ψ^*_0 space for sand-fines mixtures (up to f_c=0.30). The relation could be mathematically described by the following equation:

$$\eta_{IS} = A + \exp(-B\,\psi*) \tag{8}$$

where A and B are fitting parameters. The η_{IS} and ψ^*_0 data from this study along with experimental data for Sydney sand-fines mixtures are presented in η_{IS}-ψ^*_0 space in Fig. 18a. DEM data showed a relationship in η_{IS}-ψ^*_0 space irrespective of f_c; where A=0.910 and B=-5.19. Interestingly, the DEM simulation and experimental Sydney sand data yielded a similar trend in Fig. 18a. η_{IS} also formed a unique relationship with ψ_0, irrespective of f_c (Fig 18b), although a ψ_0<0 value was observed. However, this DEM study intended to capture only the qualitative behaviour of sand with fines and investigate the link between micro- and macro- mechanical behaviour. To match the experimental data quantitatively, alternative approaches or techniques should be considered. The performance of CN_{ss+sf} at η_{IS} ($CN_{ss+sf(IS)}$) as a measure of skeleton structure are presented in $CN_{ss+sf(IS)}$-ψ^*_0 and CN_{ss+sf}-ψ_0 spaces as shown in Fig. 18c&d. In both cases, a single correlation irrespective of f_c was obtained.

4 CONCLUSIONS

A series of constant volume (CV) triaxial compression DEM simulations were undertaken on sand-fines mixtures (f_c=0; 0.05; 0.10; 0.20) in PFC^{3D}. The influence of e_0, f_c and contact type partition on sand-fines mixtures were evaluated from a macro-mechanical and micro-mechanical standpoint. The CS and equivalent state behaviour of the mixtures were also evaluated by means of the CSL, EG-CSL as well as ψ and ψ^* which both could be correlated with characteristic features of CV behaviour. Notably, the performance and validity of e^* and its semi-empirical constituent, b, were also assessed. The key findings of the paper are listed hereafter:

i. Similar to experimental observations, when f_c remained unchanged, e_0 was shown to influence CV behaviour of sand-fines mixtures. In q-ε_q, q-p' and Δu-ε_q spaces, it was observed a larger e_0 corresponded to a more contractive response than that of a smaller e_0.

ii. In undrained shearing where e_0 is identical but f_c is increased, the CS (or overall) strength reduced. The observation aligned with the experimental supposition that for fines-in-sand soil matrixes, a meta-stable structure is formed where fines slip in between sand particles, exhibiting higher compressibility and lower q and p'. It was also observed that when fines are added to a clean sand there was a considerable reduction in CN. The finding supports the key assumption of the EST, which indicates a proportion of fines are inactive in the matrix.

iii. The average contact force at CS for three granular mixtures with varying f_c values were computed. This information along with the force chain networks of the mixtures at CS, led to the observation that the formation of strong contacts reduces with the addition of fines. When f_c=0.00, 39% of all particles were involved in strong contacts. However, for a similar initial state, when f_c=0.05 and f_c=0.10 only 5% of all particles were involved in strong contacts. The large reduction in particles involving in strong contacts suggests interlocking capabilities and force skeleton efficiency are compromised with the addition of f_c.

iv. Sand-sand contacts were observed to have a dominating contribution (>87% of total q) to the soil strength (or q) for $0 \leq f_c \leq 0.20$. Negligible contribution of fines-fines contacts to q was observed, although some sand-fines contribution was present, which increased throughout CV shearing. Therefore, a proportion of fines could be deemed active in the force transmitting structure. At larger f_c, the participation of fines to q increased, supporting the concept of e^*. On the other hand, the supposition that e_{sk} may not provide an equivalent density index at larger f_c (within f_c<f_{thre}) advances.

v. The CN, CN_{ss+sf} and Z_m was analysed for granular mixtures. Unlike for clean sand, CN did not represent the dilative tendencies of granular mixtures, which could be explained by fines floating in void spaces. Although, $CN_{ss+sf} \approx Z_m$ suggesting that mechanical contacts in granular mixtures are comprised of mainly sand-sand and sand-fine contacts, when f_c<f_{thre}. Although reportedly Z_m captures the dilative tendencies of clean sands well, this study reported CN_{ss+sf} better reflects a mechanical coordination number (i.e. stress state at CS), where fines are included.

vi. The EST was evaluated for sand-fines mixtures from a numerical perspective. Many experimental observations aligned with our numerical findings. As fines are added to the soil a downward shift in the CSL was observed in e-log p' space. In e^*- log p' space an EG-CSL was formed irrespective of f_c. ψ^* formed encouraging correlation with characteristic features of CV behaviour, i.e. η_{PT}, u_F and η_{IS}. The elegancy of the EST was therefore showcased for DEM granular material within the range of $0 \leq f_c \leq 0.20$, e.g. ψ could be replaced with ψ^* in state-dependent constitutive modelling applications.

vii. Acknowledging the original definition of b and its semi-empirical nature, a new interpretation of b was developed using stress partitions of contact types. It was observed that $e^*_{DEM} \approx e^*$ and therefore a unique EG-CSL was achieved with the new interpretation of b. The finding helps to advance the physical understanding of b and EST.

Although the study presents valuable DEM findings relating to the behaviour of granular mixtures, the application of findings to natural granular mixtures should be carefully considered. Natural granular material which generally possess coarser and finer fractions have micro-structural characteristics that may not align with DEM spheres. This study partially incorporated particle shape by using rolling resistance model whilst also considering a large enough specimen to minimize the influence of the rigid boundary. However, the results for natural granular material may diverge from the ones produced by this study.

Acknowledgement

The first author would like to acknowledge the support provided by the Research Training Program domestic (RTPd) scholarship awarded by The School of Natural and Built Environments, University of South Australia.

REFERENCES

Andrade, J., Chen, Q., Le, P., Avila, C., and Evans, T. (2012). "On the rheology of dilative granular media: bridging solid- and fluid-like behavior." *Journal of the Mechanics and Physics of Solids*, 60, 1122-1136.

ASTM D2487-17 (2017). "Standard Practice for Classification of Soils for Engineering Purposes (Unified Soil Classification System)." ASTM International, West Conshohocken, PA.

Baki, M. A. L., Rahman, M. M., and Lo, S. R. (2014). "Predicting onset of cyclic instability of loose sand with fines using instability curves." *Soil Dyn Earthq Eng*, 61–62, 140-151.

Baki, M. A. L., Rahman, M. M., Lo, S. R., and Gnanendran, C. T. (2012). "Linkage between static and cyclic liquefaction of loose sand with a range of fines contents." *Can Geotech J*, 49(8), 891-906.

Been, K., and Jefferies, M. G. (1985). "A state parameter for sands." *Geotechnique*, 35(2), 99-112.

Bobei, D. C., Lo, S. R., Wanatowski, D., Gnanendran, C. T., and Rahman, M. M. (2009). "A modified state parameter for characterizing static liquefaction of sand with fines." *Can Geotech J*, 46(3), 281-295.

Bouckovalas, G. D., Andrianopoulos, K. I., and Papadimitriou, A. G. (2003). "A critical state interpretation for the cyclic liquefaction resistance of silty sands." *Soil Dyn Earthq Eng*, 23, 115-125.

BS 5930 (2015). "Code of practice for ground investigations." British Standard UK.

Carraro, J. A. H., Prezzi, M., and Salgado, R. (2009). "Shear Strength and Stiffness of Sands Containing Plastic or Nonplastic Fines." *Journal of Geotechnical and Geoenvironmental Engineering*, 135(9), 1167-1178.

Carrera, A., Coop, M., and Lancellotta, R. (2011). "Influence of grading on the mechanical behaviour of stava tailings." *Geotechnique*, 61(11), 935-946.

Christoffersen, J., Mehrabadi, M. M., and Nemat-Nasser, S. (1981). "A Micromechanical Description of Granular Material Behavior." *Journal of Applied Mechanics*, 48(2), 339-344.

Chu, J., and Leong, W. K. (2002). "Effect of fines on instability behaviour of loose sand." *Geotechnique*, 52(10), 751-755.

Cubrinovski, M., Green, R., Allen, J., Ashford, S., Bowman, E., Bradley, B. A., Cox, B., Hutchinson, T., Kavazanjian, E., Orense, R., Pender, M., Quigley, M., and Wotherspoon, L. (2010). "Geotechnical reconnaissance of the 2010 Darfield (New Zealand) earthquake." University of Canterbury, Christchurch, 173.

Cubrinovski, M., and Ishihara, K. (2002). "Maximum and minimum void ratio characteristics of sands." *Soils Found*, 42(6), 65-78.

Cundall, P. A., and Strack, O. D. L. (1979). "A discrete numerical model for granular assemblies." *Geotechnique*, 29(1), 47-65.

Dai, B., Yang, J., and Luo, X. (2015). "A numerical analysis of the shear behavior of granular soil with fines." *Particuology*, 21, 160-172.

Fu, P., and Dafalias, Y. F. (2011). "Fabric evolution within shear bands of granular materials and its relation to critical state theory." *International Journal for Numerical and Analytical Methods in Geomechanics*, 35(18), 1918-1948.

Gao, Z., Zhao, J., Li, X.-S., and Dafalias, Y. F. (2014). "A critical state sand plasticity model accounting for fabric evolution." *International Journal for Numerical and Analytical Methods in Geomechanics*, 38(4), 370-390.

Georgiannou, V. N., Burland, J. B., and Hight, D. W. (1990). "The undrained behaviour of clayey sands in triaxial compression and extension." *Geotechnique*, 40(3), 431-449.

Gong, J., and Liu, J. (2017). "Mechanical transitional behavior of binary mixtures via DEM: Effect of differences in contact-type friction coefficients." *Computers and Geotechnics*, 85, 1-14.

Gu, X., Huang, M., and Qian, J. (2014). "DEM investigation on the evolution of microstructure in granular soils under shearing." *Granular Matter*, 16(1), 91-106.

Huang, X., Hanley, K. J., O.C ,navilluS′, and Kwok, C. (2014). "Effect of sample size on the response of DEM samples with a realistic grading." *Particuology*, 15, 107-115.

Huang, X., O'sullivan, C., Hanley, K. J., and Kwok, C. Y. (2014). "Discrete-element method analysis of the state parameter." *Geotechnique*, 954-965.

Huang, Y.-T., Huang, A.-B., Kuo, Y.-C., and Tsai, M.-D. (2004). "A laboratory study on the undrained strength of silty sand from Central Western Taiwan." *Soil Dyn Earthq Eng*, 24, 733-743.

Imam, S. M. R., Morgenstern, N. R., Robertson, P. K., and Chan, D. H. (2002). "Yielding and flow liquefaction of loose sand." *Soils Found*, 42(3), 19-31.

Iwashita, K., and Oda, M. (1998). "Rolling resistance at contacts in simulation of shear band development by DEM." *Jouranl of Engineering Mechanics*, 124, 285-292.

Jefferies, M. G. (1993). "Nor-Sand: a simple critical state model for sand." *Geotechnique*, 43(1), 91-103.

Kenney, T. C. (1977). "Residual strength of mineral mixture." *Proc. 9th International Conference of Soil Mechanics and Foundation Engineering*, 155-160.

Kuerbis, R., Negussey, D., and Vaid, Y. P. (1988). "Effect of gradation and fine content on the undrained response of sand." *Hydraulic fill structure, Geotechnical Special Publication 21, ASCE*, D. J. A. V. Zul, and S. G. Vick, eds.New York, 330-345.

Kuhn, M. R. (2006). "OVAL and OVALPLOT: Programs for analyzing dense particle assemblies with the discrete element method." 98p.

Kuhn, M. R. (2016). "The critical state of granular media: convergence, stationarity and disorder." *Geotechnique*, 0(0), 1-8.

Lade, P. V., Liggio, C. D., and Yamamuro, J. A. (1998). "Effects of non-plastic fines on minimum and maximum void ratios of sand." *Geotech Test J*, 21(4), 336-347.

Lashkari, A. (2014). "Recommendations for extension and re-calibration of an existing sand constitutive model taking into account varying non-plastic fines content." *Soil Dyn Earthq Eng*, 61–62(0), 212-238.

Li, X.-S., Dafalias, Y. F., and Wang, Z.-L. (1999). "State-dependant dilatancy in critical-state constitutive modelling of sand " *Can Geotech J*, 36(4), 599-611.

Li, X., and Dafalias, Y. (2000). "Dilatancy for cohesionless soils." *Geotechnique*, 50(4), 449-460.

Manzari, M. T., and Dafalias, Y. F. (1997). "A critical state two-surface plasticity model for sands." *Geotechnique*, 47(2), 255-272.

Marketos, G., and Bolton, M. D. (2010). "Flat boundaries and their effect on sand testing." *International journal for numerical and analytical methods in geomechanics*, 34(8), 821-837.

McGeary, R. K. (1961). "Mechanical packing of spherical particles." *J Am Ceram Soc*, 44(10), 513-522.

Minh, N., and Cheng, Y. (2014). "A micromechanical study of the equivalent granular void ratio of soil mixtures using DEM." *International Symposium on Geomechanics from Micro and Macro*, K. Soga, K. Kumar, G. Biscontin, and M. Kuo, eds., CRC Press-Taylor & Francis Group, University of Cambridge, UK, 219-224.

Mitchell, J. K. (1976). *Fundamental of soil behaviour*, Wiley, New York.

Mohammadi, A., and Qadimi, A. (2015). "A simple critical state approach to predicting the cyclic and monotonic response of sands with different fines contents using the equivalent intergranular void ratio." *Acta Geotechnica*, 1-20.

Murthy, T. G., Loukidis, D., Carraro, J. A. H., Prezzi, M., and Salgado, R. (2007). "Undrained monotonic response of clean and silty sands." *Geotechnique*, 57(3), 273-288.

Ng, T.-T., Zhou, W., and Chang, X.-L. (2016). "Effect of Particle Shape and Fine Content on the Behavior of Binary Mixture." *Journal of Engineering Mechanics*, 143(1).

Ng, T. (2006). "Input Parameters of Discrete Element Methods." *Journal of Engineering Mechanics*, 132(7), 723-729.

Nguyen, H. B. K., Rahman, M. M., and Fourie, A. B. (2017). "Undrained behaviour of granular material and the role of fabric in isotropic and K0 consolidations: DEM approach." *Geotechnique*, 67(2), 153-167.

Nguyen, H. B. K., Rahman, M. M., and Fourie, A. B. (2018). "Characteristic behavior of drained and undrained triaxial compression tests: DEM study." *Journal of Geotechnical and Geoenvironmental Engineering*, 144(9), 1-13.

Ni, Q., Tan, T. S., Dasari, G. R., and Hight, D. W. (2004). "Contribution of fines to the compressive strength of mixed soils." *Geotechnique*, 54(9), 561-569.

Papadopoulou, A., and Tika, T. (2008). "The Effect of Fines on Critical State and Liquefaction Resistance Characteristics of Non-Plastic Silty Sands." *Soils Found*, 48(5), 713-725.

Perez, J. C. L., Kwok, C. Y., O'Sullivan, C., Huang, X., and Hanley, K. J. (2016). "Exploring the micro-mechanics of triaxial instability in granular materials." *Geotechnique*, 1-16.

Pitman, T. D., Robertson, P. K., and Sego, D. C. (1994). "Influence of fines on the collapse of loose sands." *Can Geotech J*, 31(5), 728-739.

Qadimi, A., and Coop, M. R. (2007). "The undrained cyclic behaviour of a carbonate sand." *Geotechnique*, 57(9), 739-750.

Rabbi, A. T. M. Z., Rahman, M. M., and Cameron, D. A. (2019). "Instability of natural silty sand under undrained and constant shear drained path : A critical state study." *International Journal of Geomechanics*, 19(8), 04019083.

Radjai, F., Wolf, D. E., Jean, M., and Moreau, J. (1998). "Bimodal character of stress transmission in granular packings." *Phys. Rev. Lett* 80(1), 61-64.

Rahman, M., Baki, M., and Lo, S. (2014). "Prediction of Undrained Monotonic and Cyclic Liquefaction Behavior of Sand with Fines Based on the Equivalent Granular State Parameter." *International Journal of Geomechanics*, 14(2), 254-266.

Rahman, M., Khayyer, F., and Karim, R. (2017). "Discussion of "Effect of particle shape and fine content on the behavior of binary mixture" " *Journal of Engineering Mechanics*, 143(9), 07017003.

Rahman, M. M. (2009). "Modelling the influence of fines on liquefaction behaviour."PhD Thesis, University of New South Wales at Australian Defence Force Academy, Canberra, Australia.

Rahman, M. M., Lo, S.-C. R., and Dafalias, Y. F. (2014). "Modelling the static liquefaction of sand with low-plasticity fines." *Geotechnique*, 64(11), 881-894.

Rahman, M. M., and Lo, S. R. (2007). "Equivalent granular void ratio and state parameters for loose clean sand with small amount of fines." *10th Australia New Zealand Conference on Geomechanics: Common Ground*Brisbane, Australia, 674-679.

Rahman, M. M., and Lo, S. R. (2008). "The prediction of equivalent granular steady state line of loose sand with fines." *Geomechanics and Geoengineering*, 3(3), 179 - 190.

Rahman, M. M., and Lo, S. R. (2012). "Predicting the onset of static liquefaction of loose sand with fines." *Journal of Geotechnical and Geoenvironmental Engineering*, 138(8), 1037-1041.

Rahman, M. M., and Lo, S. R. (2014). "Undrained behaviour of sand-fines mixtures and their state parameters." *Journal of Geotechnical and Geoenvironmental Engineering*, 140(7).

Rahman, M. M., Lo, S. R., and Baki, M. A. L. (2011). "Equivalent granular state parameter and undrained behaviour of sand-fines mixtures." *Acta Geotechnica*, 6(4), 183-194.

Rahman, M. M., Lo, S. R., and Gnanendran, C. T. (2008). "On equivalent granular void ratio and steady state behaviour of loose sand with fines." *Can Geotech J*, 45(10), 1439-1455.

Rahman, M. M., Lo, S. R., and Gnanendran, C. T. (2009). "Reply to discussion by Wanatowski, D. and Chu, J. on- On equivalent granular void ratio and steady state behaviour of loose sand with fines." *Can Geotech J*, 46(4), 483-486.

Rahman, M. M., Nguyen, H. B. K., and Rabbi, A. T. M. Z. (2018). "The effect of consolidation on undrained behaviour of granular materials: experiment and DEM simulation." *Geotechnical Research*, 5(4), 199-217.

Rahman, M. M., and Sitharam, T. G. (2019). "Cyclic liquefaction screening of sand with non-plastic fines: Critical state approach." *Geoscience Frontiers*.

Rothenburg, L., and Bathurst, R. J. (1989). "Analytical study of induced anisotropy in idealized granular materials." *Geotechnique*, 39(4), 601-614.

Shen, C. K., Vrymoed, J. L., and Uyeno, C. K. (1977). "The effect of fines on liquefaction of sands." *The 9th International Conference on Soil Mechanics and Foundation Engineering*Tokyo, 381-385.

Shire, T., O'Sullivan, C., and Hanley, K. J. (2016). "The influence of fines content and size-ratio on the micro-scale properties of dense bimodal materials." *Granular Matter*, 18(3), 1-10.

Sitharam, T. G., Vinod, J. S., and Ravishankar, B. V. (2008). "Evaluation of undrained response from drained triaxial shear tests: DEM simulations and experiments." *Geotechnique*, 58(7), 605-608.

Sitharam, T. G., Vinod, J. S., and Ravishankar, B. V. (2009). "Post-liquefaction undrained monotonie behaviour of sands: Experiments and DEM simulations." *Geotechnique*, 59(9), 739-749.

Skempton, A. W., and Brogan, J. M. (1994). "Experiments on piping in sandy gravels." *Geotechnique*, 44, 449-460.

Sukumaran, B., Leonards, G. A., and Fox, J. P. (1996). "Discussion: Liquefaction and Postliquefaction Behaviour of Sand." *Journal of Geotechnical and Geoenvironmental Engineering*, 122(6), 502-503.

Thevanayagam, S., Ravishankar, K., and Mohan, S. (1997). "Effects of fines on monotonic undrained shear strength of sandy soils." *Geotech Test J*, 20(4), 394-406.

Thevanayagam, S., Shenthan, T., Mohan, S., and Liang, J. (2002). "Undrained fragility of clean sands, silty sands, and sandy silts." *Journal of Geotechnical and Geoenvironmental Engineering*, 128(10), 849-859.

Thornton, C. (2000). "Numerical simulations of deviatoric shear deformation of granular media." *Geotechnique*, 50(1), 43-53.

Troncoso, J. H., and Verdugo, R. (1985). "Silt content and dynamic behaviour of tailing sands." *Proc. 11th International Conference on Soil Mechanics and Foundation Engineering*, 1311-1314.

Yamamuro, J. A., and Lade, P. V. (1998). "Steady-State Concepts and Static Liquefaction of Silty Sands." *Journal of Geotechnical and Geoenvironmental Engineering*, 124(9), 868-877.

Yan, W., and Dong, J. (2011). "Effect of Particle Grading on the Response of an Idealized Granular Assemblage." *International Journal of Geomechanics*, 11(4), 276-285.

Yang, J. (2002). "Non-uniqueness of flow liquefaction line for loose sand." *Geotechnique*, 52(10), 757-760.

Yang, J., Liu, X., Guo, Y., and Liang, L. B. (2018). "A unified framework for evaluating in situ state of sand with varying fines content." *Geotechnique*, 68(2), 177-183.

Yang, J., Wei, L. M., and Dai, B. B. (2015). "State variables for silty sands: Global void ratio or skeleton void ratio?" *Soils Found*, 55(1), 99-111.

Yin, Z.-Y., Zhao, J., and Hicher, P.-Y. (2014). "A micromechanics-based model for sand-silt mixtures." *International Journal of Solids and Structures*, 51(6), 1350-1363.

Yoshimine, M., and Ishihara, k. (1998). "Flow potential of sand during liquefaction." *Soils Found*, 38(3), 189-198.

Zhang, J., Lo, S. C. R., Rahman, M. M., and Yan, J. (2018). "Characterizing monotonic behaviour of pond ash within critical state approach." *Journal of Geotechnical and Geoenvironmental Engineering*, 144(1).

Zhao, J., and Guo, N. (2013). "Unique critical state characteristics in granular media considering fabric anisotropy." *Geotechnique*, 695-704.

Zhou, W., Wu, W., Ma, G., Huang, Y., and Chang, X. (2017). "Study of the effects of anisotropic consolidation on granular materials under complex stress paths using the DEM." *Granular Matter*, 19(4), 1-15.

Zhou, W., Wu, W., Ma, G., Ng, T.-T., and Chang, X. (2018). "Undrained behavior of binary granular mixtures with different fines contents." *Powder Technology*, 340, 139-153.

Zhou, W., Xu, K., Ma, G., Yang, L., and Chang, X. (2016). "Effects of particle size ratio on the macro- and microscopic behaviors of binary mixtures at the maximum packing efficiency state." *Granular Matter*, 18(4), 1-13.

Zlatovic, S., and Ishihara, K. (1995). "On the influence of nonplastic fines on residul strength." *Proceedings of IS-TOKY0'95/ The First International Conference on Earthquake Geotechnical Engineering/Tokyo/ 14-16 November 1995*, K. Ishihara, ed., A.A. Balkema, Rotterdam, Tokyo, Japan, 239-244.

APPENDIX

Equivalent granular void ratio, *e**

Rahman and Lo (2008), by re-analysing the experimental data of McGeary (1961) on binary packing studies and nine different sand-fines mixture from around the world, concluded that b entering Eq.(1) is a function of both f_c and $\chi = D_s/d_f$, where D_s is the characteristic size of sand and d_f is the characteristic size of fines. Furthermore, the functional relationship, $b = F(f_c, \chi)$, has to possess a number of mathematical attributes (Rahman et al. 2008). To simulate the required attributes, Rahman and Lo (2008) proposed a semi-empirical equation expressed as below.

$$b = \left[1 - \exp\left(-0.3\frac{\left(f_c / f_{thre}\right)}{k}\right)\right] \times \left(r\frac{f_c}{f_{thre}}\right)^r \qquad \text{(A1)}$$

where $r = \chi^{-1}$= particle size ratio, d_f/D_s and $k = 1 - r^{0.25}$. Since sand and fines are generally not single-size materials, D_s/d_f was generalized to $D_{s,10}/d_{f,50}$ based on the argument in Ni et al. (2004), where the subscripts denote fractile passing. f_{thre} can be obtained from the experimental data, where available, as outlined in Rahman et al. (2009). However, as an initial approximation, f_{thre} can be taken as 0.30, but it may be determined more reliably using the following equation developed by Rahman *et al*. (2009).

$$f_{thre} = 0.40\left(\frac{1}{1 + e^{\alpha - \beta\chi}} + \frac{1}{\chi}\right) \qquad \text{(A2)}$$

The parameters α and β are determined by curve fitting to eight databases for χ in the range of 2 to 42, and this gave $\alpha = 0.50$ and $\beta = 0.13$.

Notations

Δu:	excess pore water pressure
ε:	strain rate
ε_q:	deviatoric strain
ε_v:	volumetric strain
η_{IS}:	stress ratio at instability state
η_{PT}:	stress ratio at phase transformation
λ:	slope of CSL in e-log p' space
μ:	inter-particle friction coefficient
μ_r:	rolling resistance coefficient
ξ:	CSL fitting parameter in e-log p' space
σ_1:	maximum principal stress
σ_3:	minor principal stress
ψ:	state parameter
ψ_0:	state parameter at the beginning of shearing
ψ^*:	equivalent granular state parameter
ψ^*_0:	equivalent granular state parameter at the beginning of shearing
χ:	particle size ratio between sand and fine particles
ω_{avg}:	average angular velocity
b:	active proportion of fines in force transmitting skeleton
b':	active proportion of fines in force transmitting skeleton (obtained via DEM)
C:	total number of contacts
CN:	coordination number
$CN_{f\text{-}f}$:	coordination number for fine-fine contacts
$CN_{s\text{-}f}$:	coordination number for sand-fine contacts
$CN_{s\text{-}s}$:	coordination number for sand-sand contacts
e:	void ratio
e_0:	post-consolidation void ratio
e^*:	equivalent granular void ratio
e^*_0:	post-consolidation equivalent granular void ratio
e^*_{DEM}:	equivalent granular void ratio (obtained via b' & DEM)
e_{lim}:	CSL fitting parameter in e-log p' space
f_c:	fine content
f_{thre}:	threshold fine content
M:	slope of CSL in q-p' space
m:	flow rule fitting parameter
N:	total number of particles
p':	mean effective confining stress
p'_0:	post-consolidation mean effective confining stress
p'_{PT}:	mean effective confining stress at phase transformation
$p'_{f\text{-}f}$:	mean effective confining stress for fine-fine contacts
$p'_{s\text{-}f}$:	mean effective confining stress for sand-fine contacts
$p'_{s\text{-}s}$:	mean effective confining stress for sand-sand contacts
q:	deviatoric stress
q_{peak}:	deviatoric stress at instability state
$q_{f\text{-}f}$:	deviatoric stress for fine-fine contacts
$q_{s\text{-}f}$:	deviatoric stress for sand-fine contacts
$q_{s\text{-}s}$:	deviatoric stress for sand-sand contacts

u_F: flow potential

List of tables

Table 1. Summary of input parameters used in study.

Parameter	Value
Particle density (ρ_g)	2650kg/m^3
Effective Young's modulus (E*)	50MPa
Ratio between normal and tangential contact stiffness, (k*)	1
Inter-particle sliding friction coefficient (μ)	0.5
Rolling friction coefficient (μ_r)	0.3
Wall friction coefficient	0
Wall stiffness	1×10^{10} kN/m
Damping constant	0.7

Table 2. Summary of undrained triaxial tests used in study.

Test	μ_{sp}	f_c	N	N_s	N_f	ε (1/s)	p'_0 (kPa)	e_0	e^*	e_{sk}	*Flow type*	b	b'
T1	0.90	0	10506	10506	-	0.001	96	0.867	0.867	0.867	F	0	0
T2	0.01	0	10506	10506	-	0.001	96	0.597	0.597	0.597	NF	0	0
T3	0.50	0	10506	10506	-	0.001	96	0.838	0.838	0.838	LF	0	0
T4	0.10	0	10506	10506	-	0.001	96	0.667	0.667	0.667	NF	0	0
T5	0.20	0	10506	10506	-	0.001	96	0.726	0.726	0.726	NF	0	0
T6	0.54	0	10506	10506	-	0.001	96	0.852	0.852	0.852	F	0	0
T7	0.34	0	10506	10506	-	0.001	96	0.796	0.796	0.796	NF	0	0
T10	0.12	0	10506	10506	-	0.001	96	0.675	0.675	0.675	NF	0	0
T11	0.00	0	10506	10506	-	0.001	333	0.547	0.547	0.547	NF	0	0
T12	0.20	0	10506	10506	-	0.001	96	0.726	0.726	0.726	NF	0	0
T13	0.70	0	10506	10506	-	0.001	96	0.875	0.875	0.875	F	0	0
T14	0.34	0	10506	10506	-	0.001	96	0.796	0.796	0.796	NF	0	0
T15	0.95	0	10506	10506	-	0.001	500	0.746	0.746	0.746	NF	0	0
T16	0.60	0	10506	10506	-	0.001	500	0.742	0.742	0.742	NF	0	0
T17	0.44	0	10506	10506	-	0.001	500	0.722	0.722	0.722	NF	0	0
T18	0.01	0	10506	10506	-	0.001	96	0.597	0.597	0.597	NF	0	0
T-RR4	0.01	0	10506	10506	-	0.001	96	0.599	0.599	0.599	NF	0	0
T-RR5	0.70	0	10506	10506	-	0.001	96	0.874	0.874	0.874	F	0	0
T-RR26	0.01	0	10506	10506	-	0.001	100	0.599	0.599	0.599	NF	0	0
T-RR54	0.55	0	10506	10506	-	0.001	76	0.853	0.853	0.853	F	0	0
T-RR55	0.65	0	10506	10506	-	0.001	100	0.859	0.859	0.859	LF	0	0
T300	0.10	0.05	66020	2649	63371	0.001	94	0.626	0.705	0.712	NF	0.072	0.023
T301	0.35	0.05	66020	2649	63371	0.001	94	0.765	0.851	0.858	T	0.072	0.029
T303	0.70	0.05	66020	2649	63371	0.001	94	0.567	0.643	0.649	NF	0.072	0.022
T304	0.45	0.05	66020	2649	63371	0.001	94	0.812	0.900	0.907	F	0.072	0.033
T306	0.50	0.05	66020	2649	63371	0.001	94	0.817	0.905	0.913	F	0.072	0.032
T319	0.20	0.05	66020	2649	63371	0.001	350	0.732	0.816	0.823	T	0.072	0.024
T320	0.30	0.05	66020	2649	63371	0.001	500	0.655	0.736	0.742	NF	0.072	0.021
RT321	0.20	0.05	66020	2649	63371	0.001	100	0.685	0.767	0.773	NF	0.072	0.022
T307	0.10	0.10	129266	2524	126742	0.001	94	0.545	0.688	0.717	NF	0.151	0.051
T308	0.10	0.10	129266	2524	126742	0.0004	94	0.546	0.689	0.718	NF	0.151	0.095
T309	0.40	0.10	129266	2524	126742	0.001	94	0.711	0.870	0.901	LF	0.151	0.068
T310	0.50	0.10	144506	2809	141697	0.001	94	0.549	0.693	0.721	NF	0.151	0.150

T311	0.30	0.10	129266	2524	126742	0.001	94	0.677	0.8217	0.863	NF	0.151	0.075
T312	0.50	0.10	129266	2524	126742	0.001	94	0.746	0.908	0.940	F	0.151	0.051
RT313	0.50	0.10	129266	2524	126742	0.001	330	0.665	0.820	0.850	T	0.151	0.064
RT314	0.10	0.10	129266	2524	126742	0.001	330	0.510	0.650	0.678	NF	0.151	0.051
RT322	0.40	0.10	129266	2524	126742	0.001	500	0.602	0.751	0.780	NF	0.151	0.064
RT323	0.10	0.10	129266	2524	126742	0.001	500	0.486	0.624	0.651	NF	0.151	0.052
T315	0.10	0.20	255726	2241	253485	0.001	340	0.399	0.628	0.749	NF	0.296	0.122
T316	0.50	0.20	255726	2241	253485	0.001	96	0.620	0.886	1.025	F	0.296	0.297
T317	0.30	0.20	255726	2241	253485	0.001	100	0.635	0.903	1.044	F	0.296	0.199
RT318	0.30	0.20	255726	2241	253485	0.001	350	0.550	0.804	0.938	F	0.296	0.364
RT315	0.10	0.20	255726	2241	253485	0.001	100	0.428	0.662	0.785	NF	0.296	0.129

**Note: T behaviour denotes a transitional behaviour between NF & LF or F & LF*

Table 3. Participation of fine and sand particles to strong contact force network.

Parameter	f_c	**Proportion of fine particles in strong contact at CS**	**Proportion of sand particles in strong contact at CS**	**Proportion of particles in strong contact at CS**
T10	0.00	-	0.39	0.39
RT321	0.05	0.01	0.92	0.05
T311	0.10	0.03	0.93	0.05

List of Figures

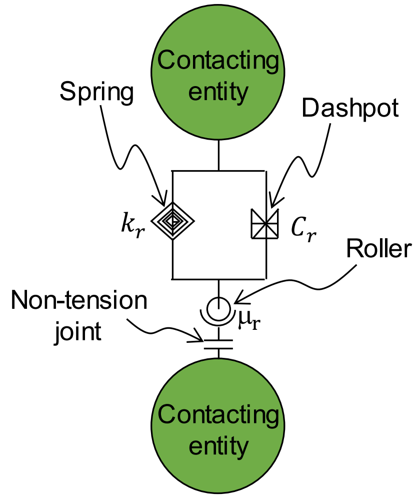

Fig. 1. Rolling rheology installed at the contact.

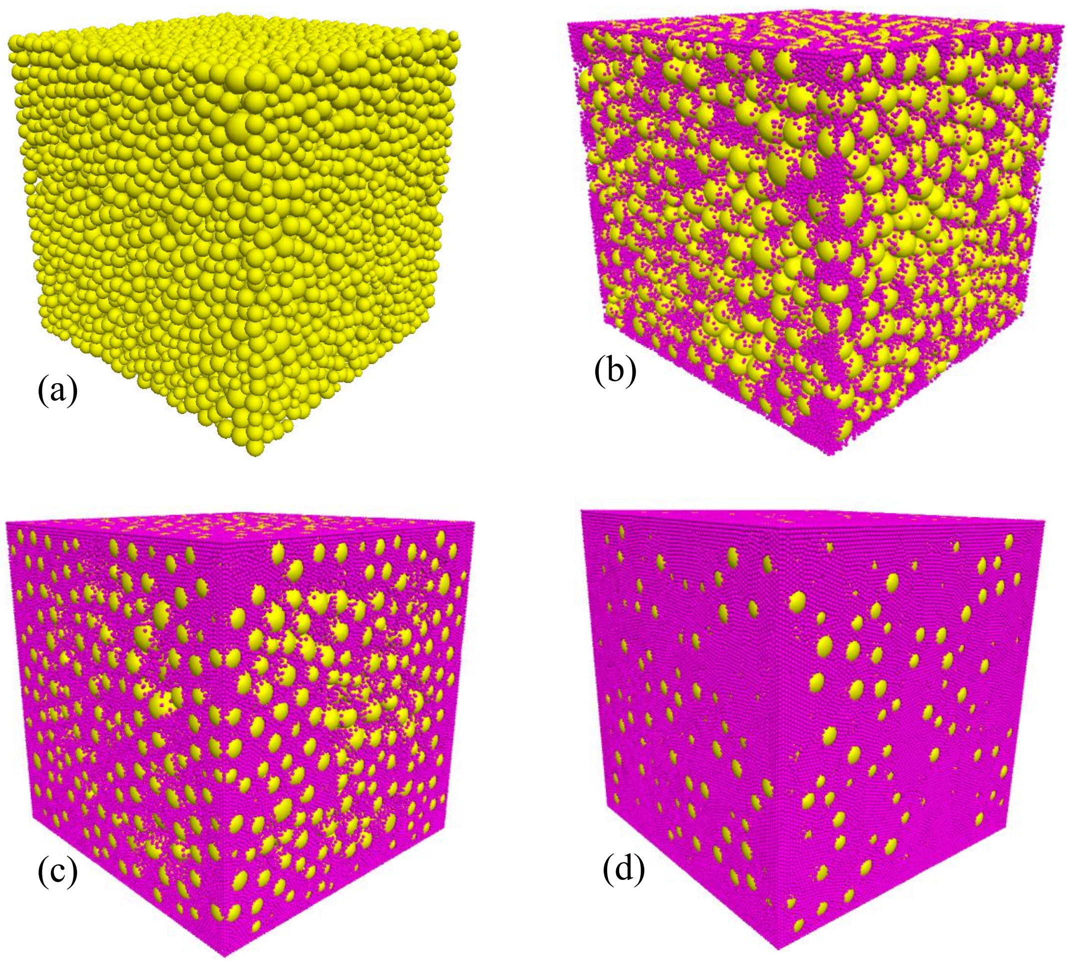

Fig. 2. DEM assemblies used in this study: (a) f_c=0.00; (b) f_c=0.05; (c) f_c=0.10; (d) f_c=0.20.

Figure 3, 4,5 & 6

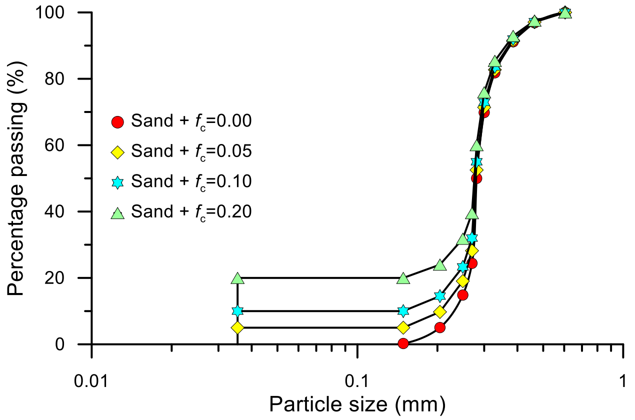

Fig. 3. Particle size distribution for studied sand and fines.

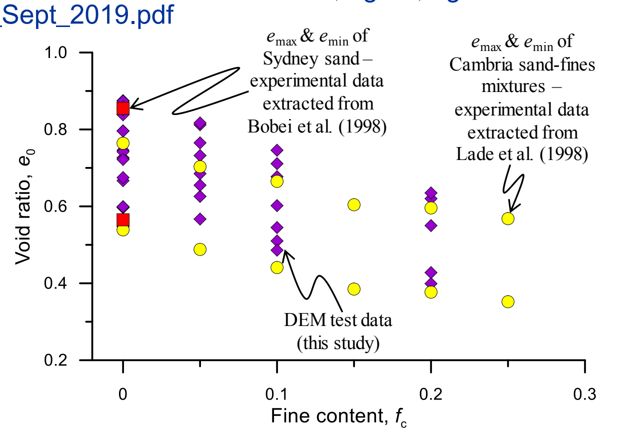

Fig. 4. Range of fine contents and void ratios considered in study.

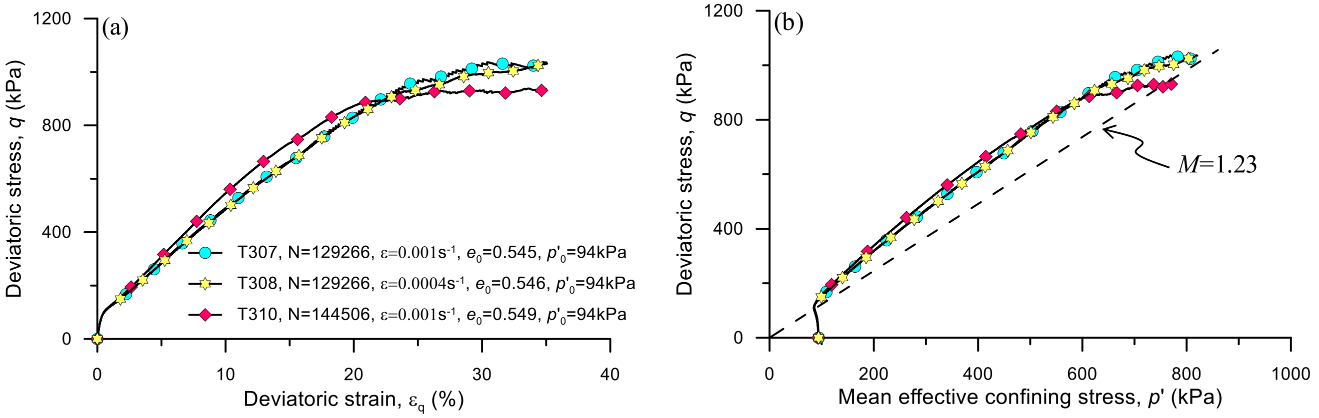

Fig. 5. Effect of specimen size and strain rate for sand with f_c=0.10 granular mixture in (a) q-ε_q and (b) q-p' spaces.

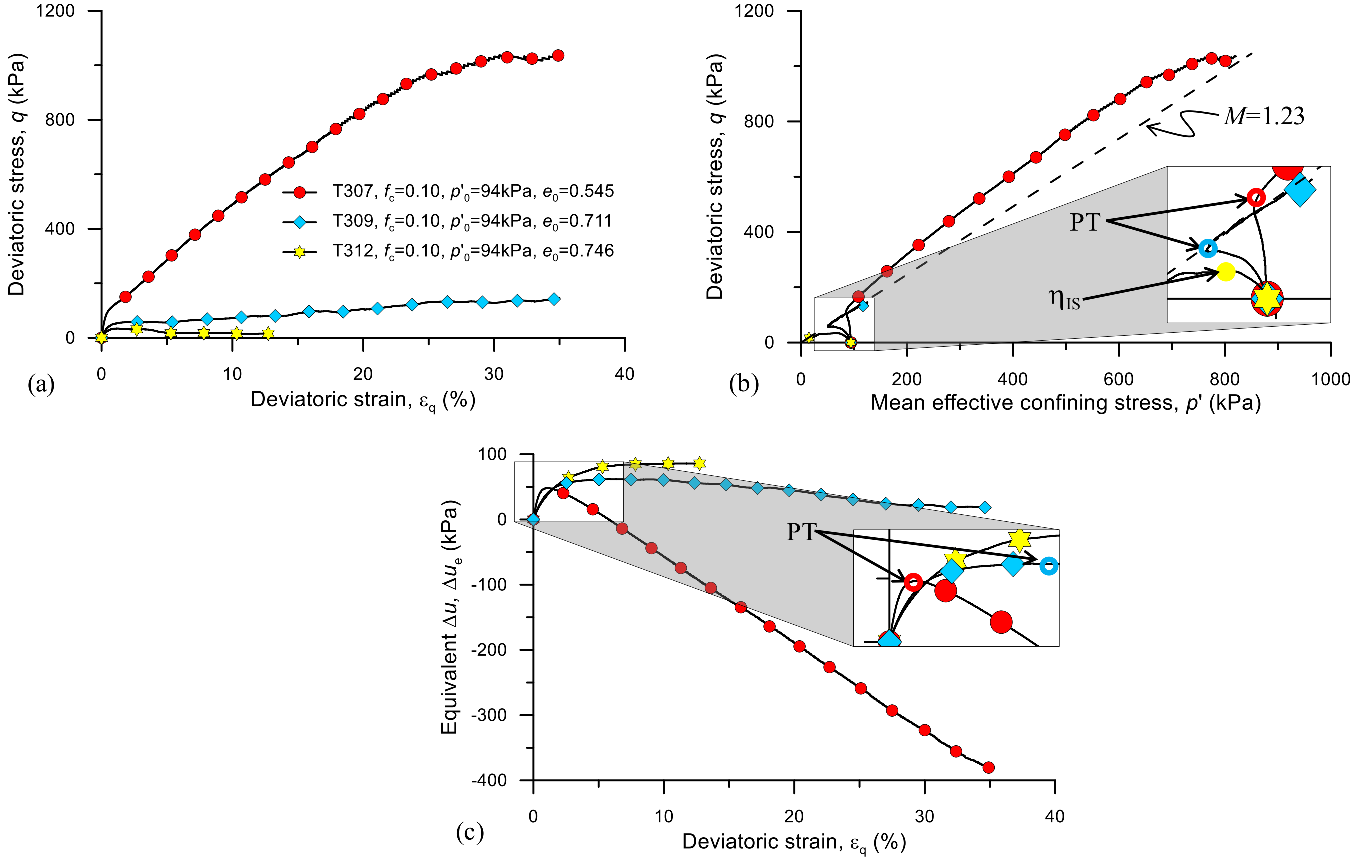

Fig. 6. Effect of e on sand with f_c=0.10 behaviour in (a) q-ε_q, (b) q-p' and (c) Δu_e-ε_q spaces.

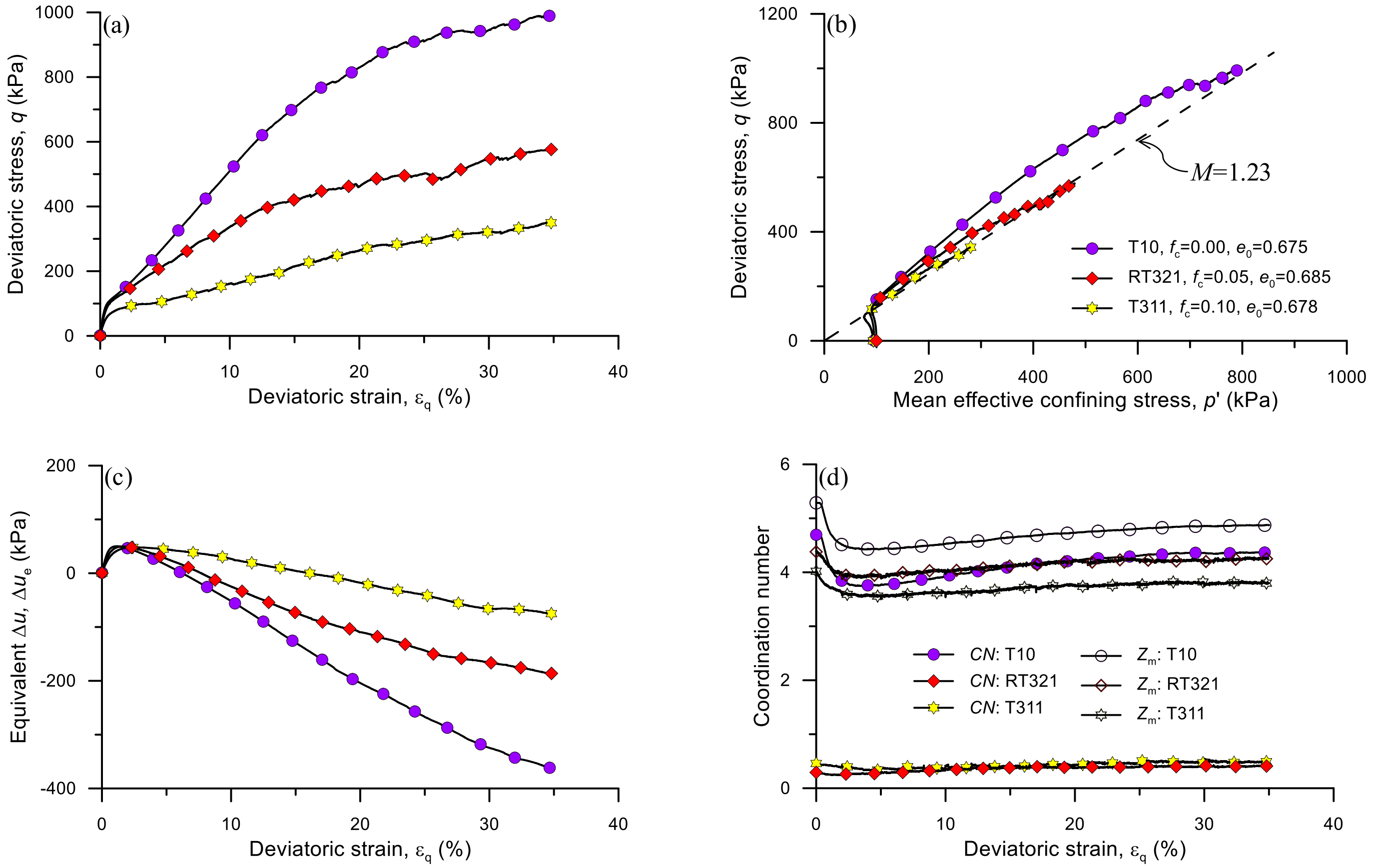

Fig. 7. Influence of f_c on undrained behaviour in (a) q-ε_q, (b) q-p' (c) Δu_e-ε_q and (d) CN/Z_m-ε_q spaces.

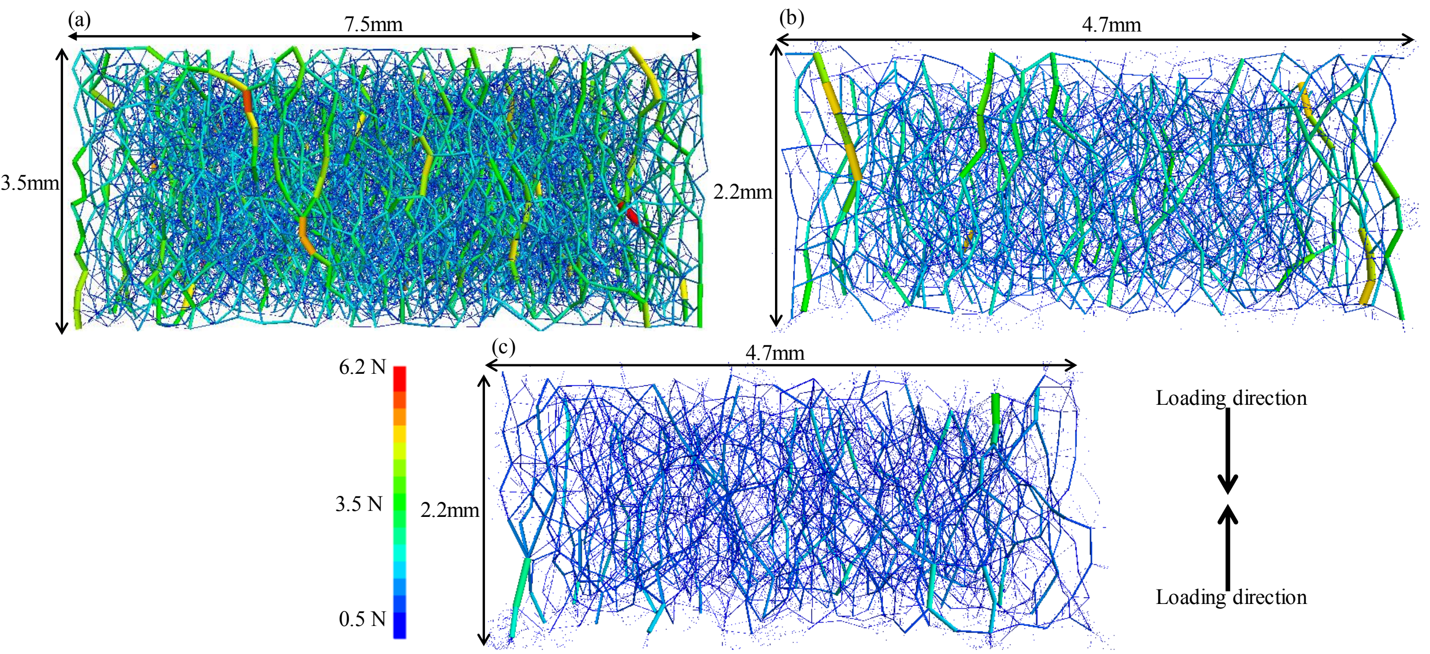

Fig. 8. Influence of the addition of fines on the force skeleton structure: (a) T10, f_c=0.00; (b) RT321, f_c=0.05; (c) T311, f_c=0.10.

Figure 9 & 10

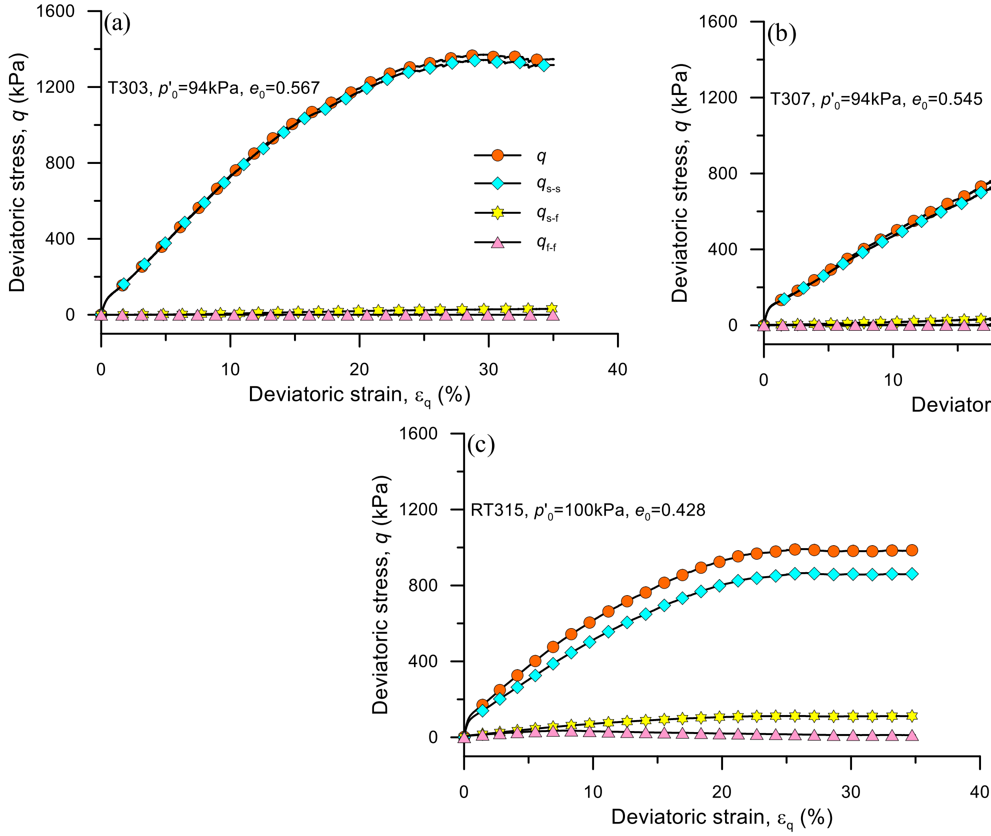

Fig. 9. The mechanical participation of each contact type in q-ε_q space for; (a) f_c=0.05; (b) f_c=0.10; (c) f_c=0.20.

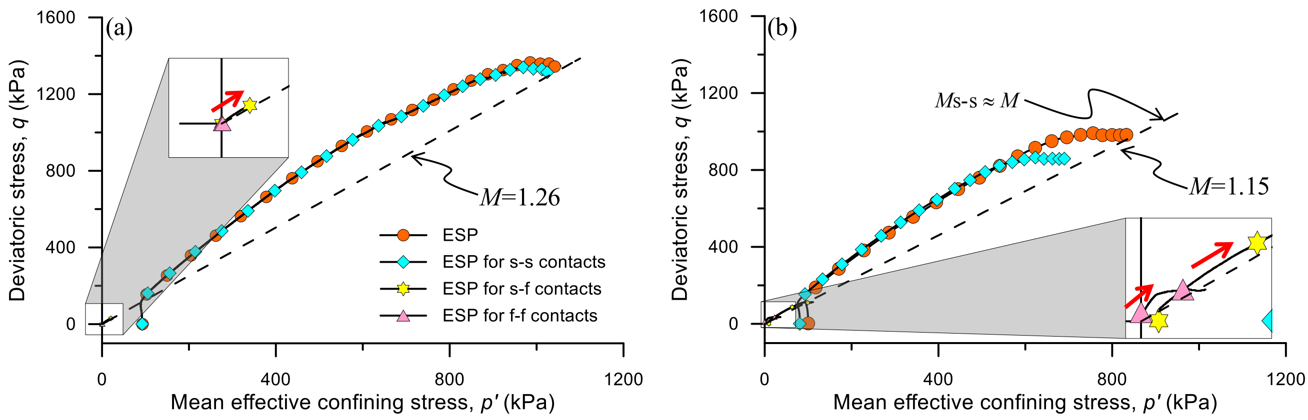

Fig. 10. The mechanical participation of each contact type in q-p' space for; (a) T303, f_c=0.05; (b) RT315, f_c=0.20.

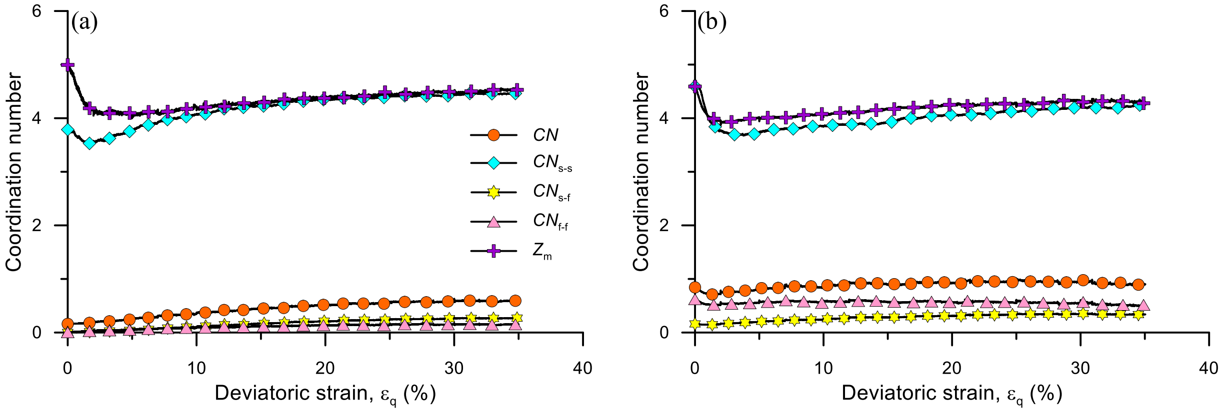

Fig. 11. Evolution of contact density for different contact types: (a) T303, f_c=0.05; (b) T307, f_c=0.10.

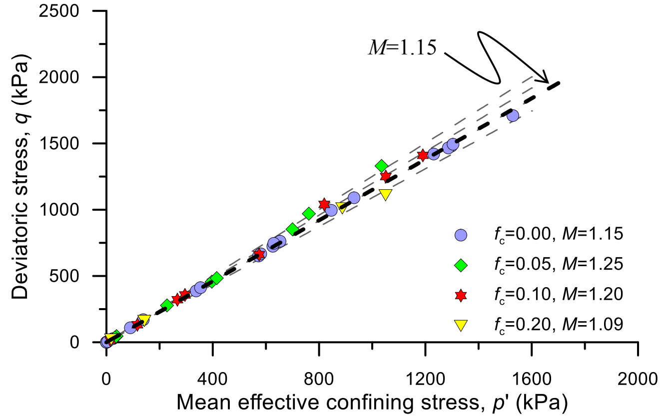

Fig. 12. CSL in q-p' space.

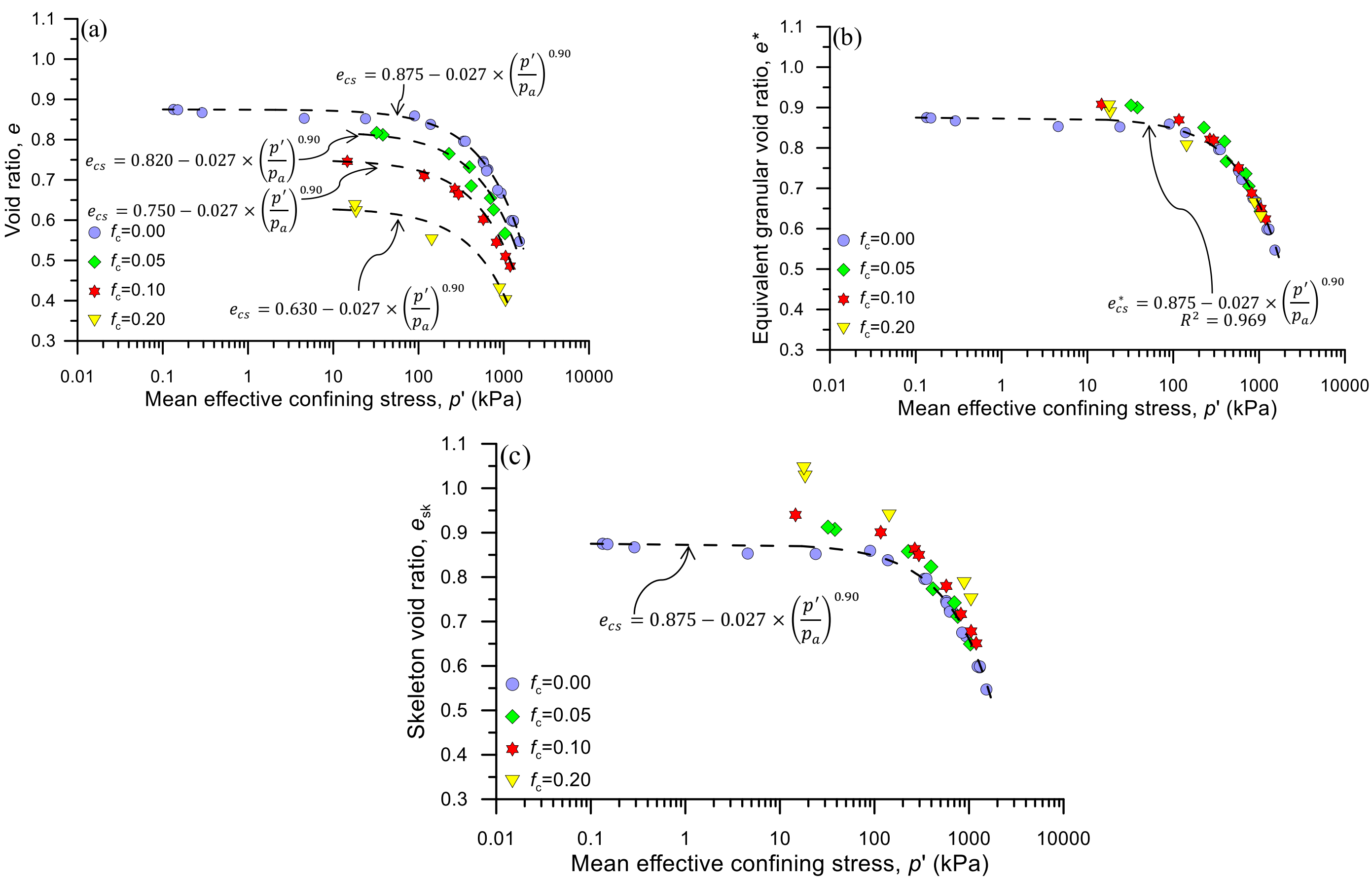

Fig. 13. CSL in for studied granular mixtures in (a) e-log p', (b) e^*-log p' and (c) e_{sk}-log p' spaces.

Figure 14 & 15

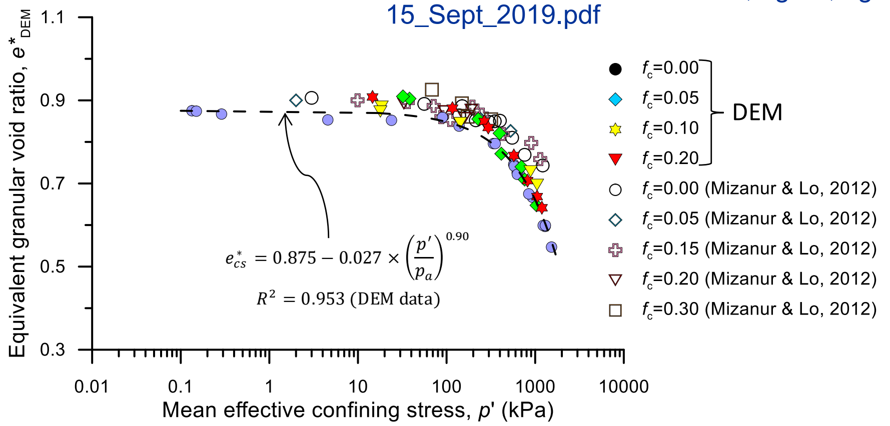

Fig. 14. The EG-CSL with e^*_{DEM} data points.

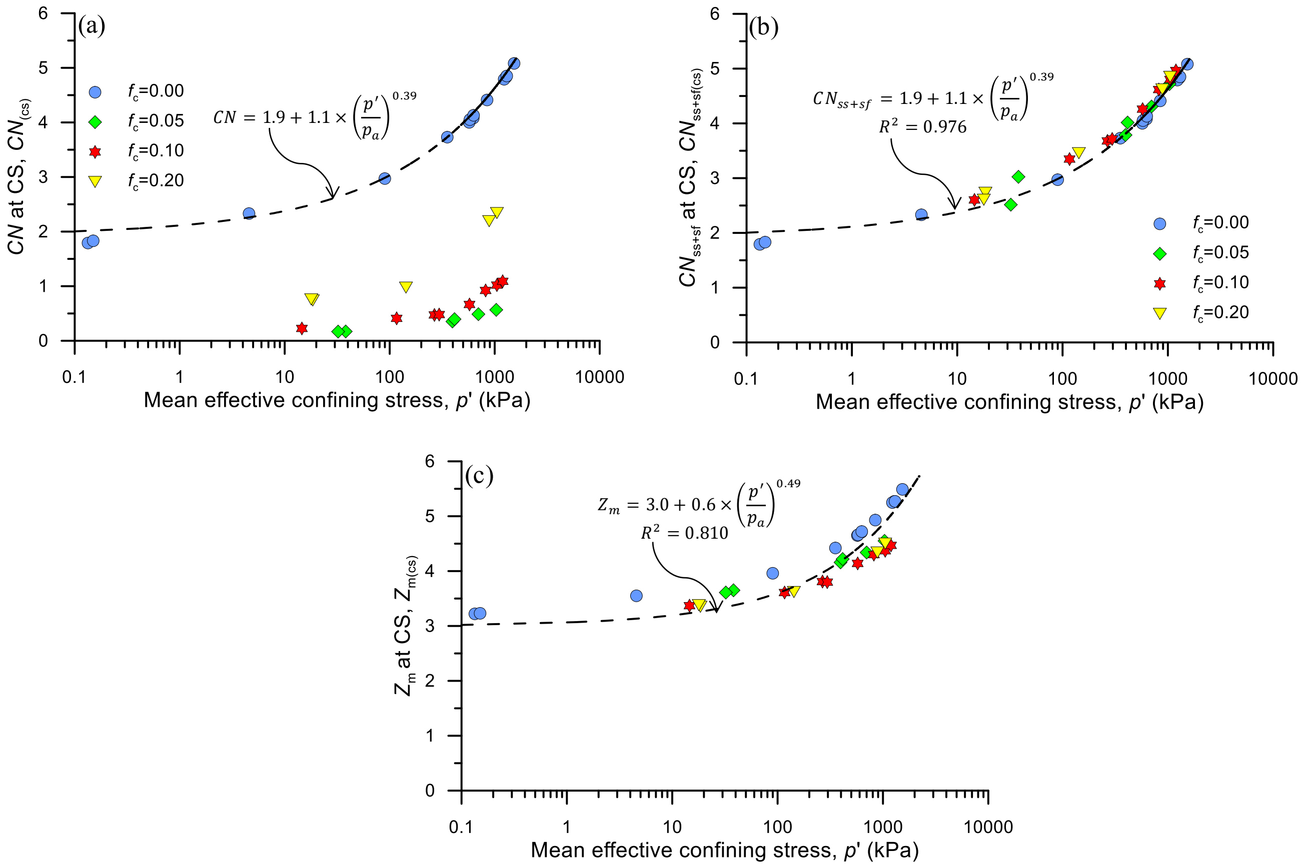

Fig. 15. The relation between coordination number and critical state stress in (a) CN-p'_{cs}, (b) CN_{ss+sf}-p'_{cs}(c) Z_{m}-p'_{cs} spaces.

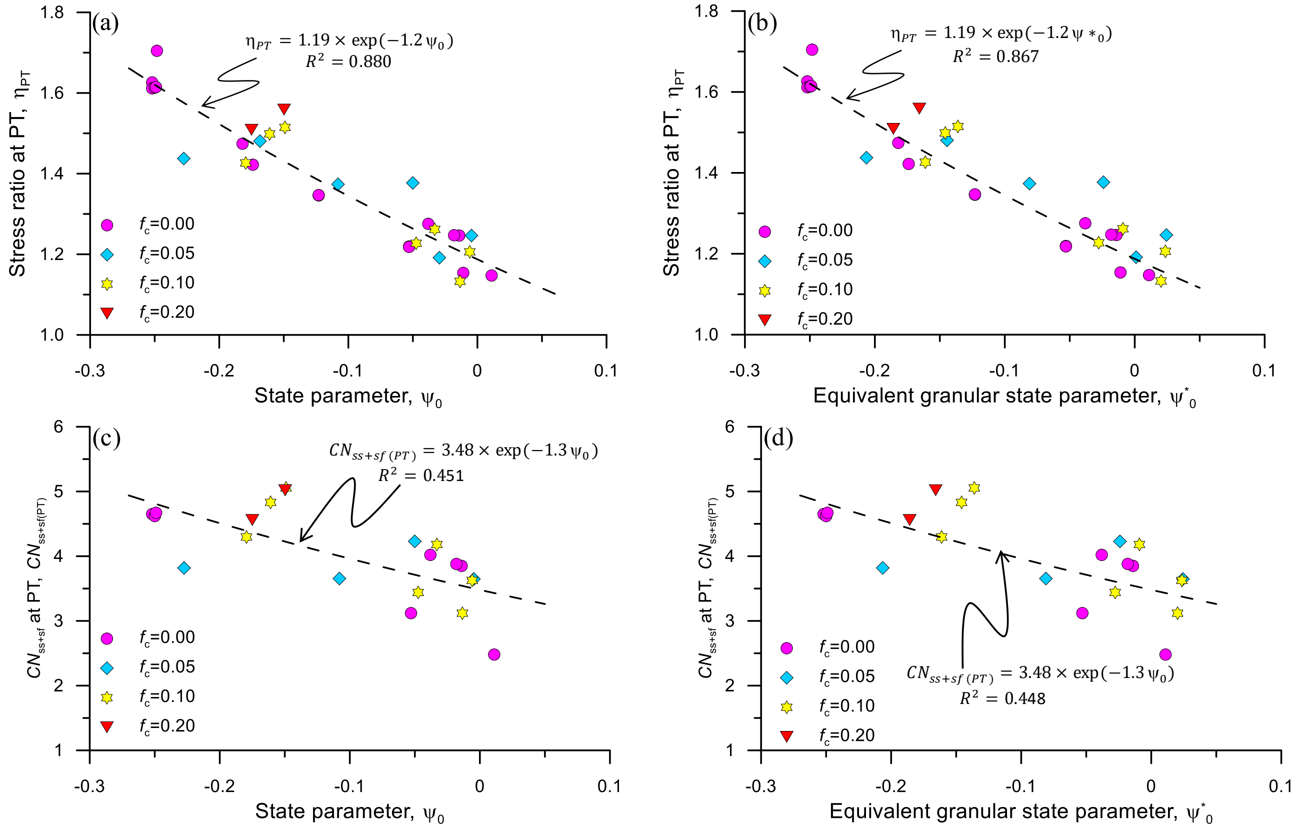

Fig. 16. The performance of ψ & ψ* capturing characteristic features at PT in (a) η_{PT}-ψ_0, (b) η_{PT}-ψ^*_0, (c) $CN_{ss+sf(PT)}$-ψ_0 and (d) $CN_{ss+sf(PT)}$-ψ^*_0 spaces.

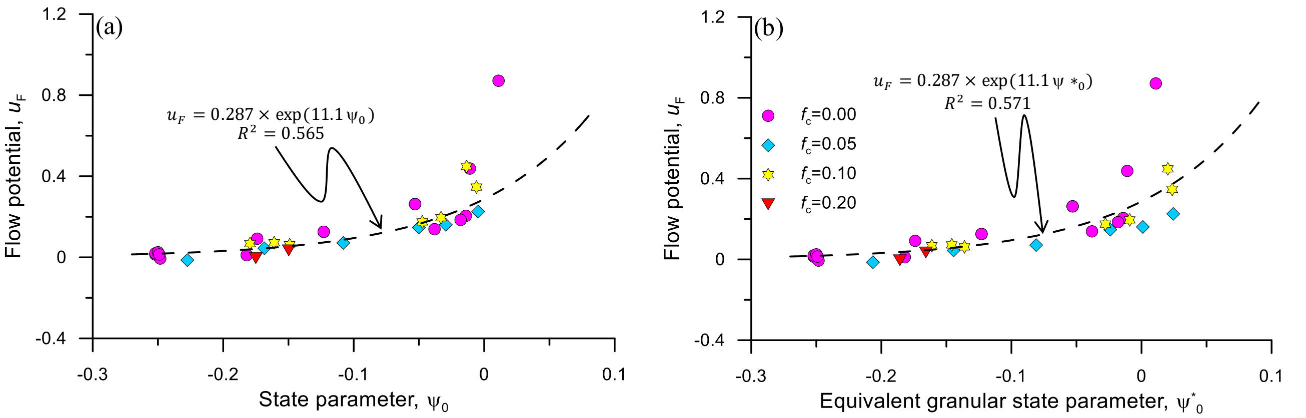

Fig. 17. The performance of ψ & ψ* capturing the flow potential of granular mixtures in (a) u_F-ψ_0 and (b) u_F-ψ^*_0 spaces.

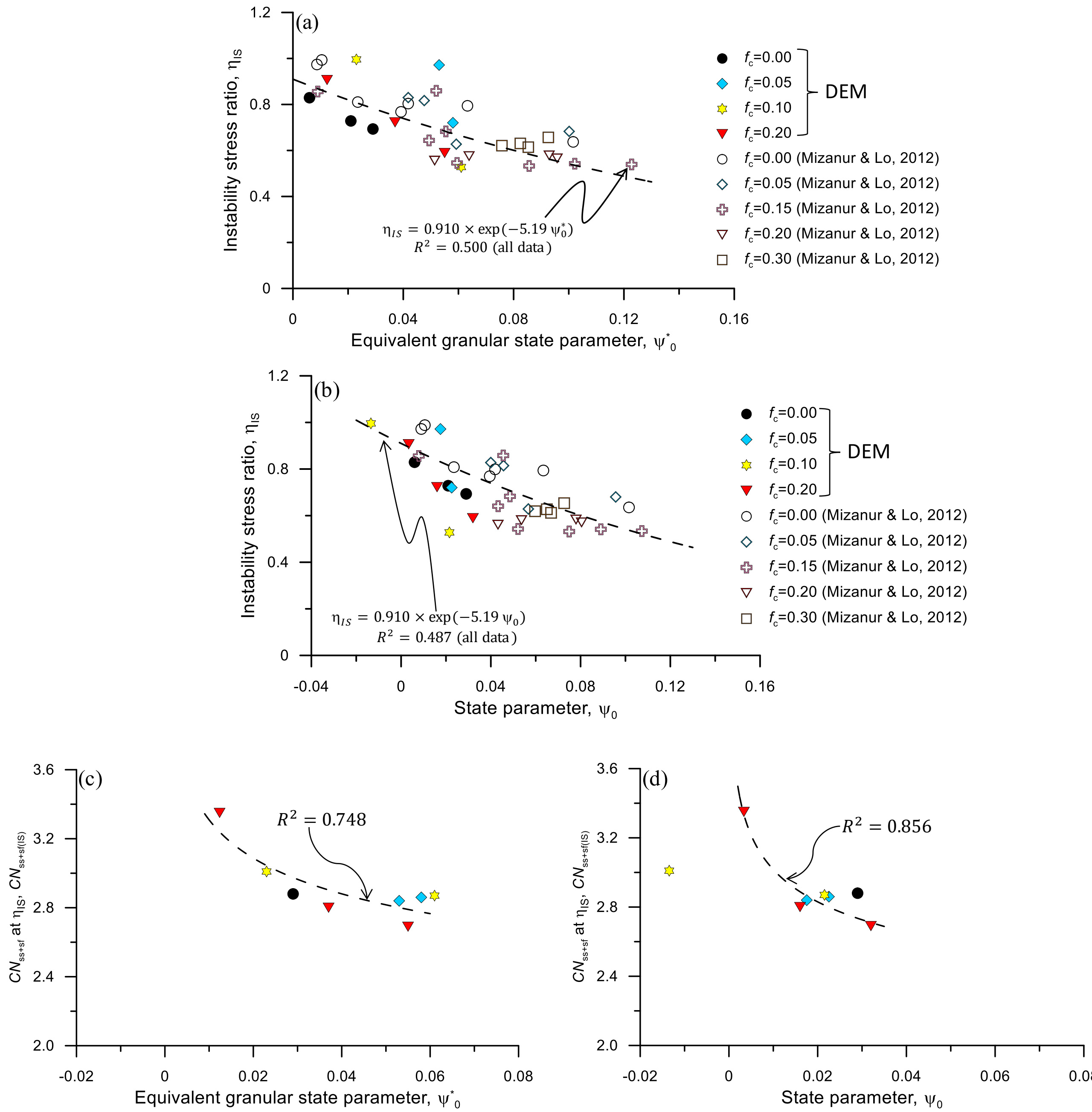

Fig. 18. The performance of ψ & ψ^* capturing undrained instability behaviour in (a) η_{IS}-ψ^*_0, (b) η_{IS}-ψ_0, (c) $CN_{ss+sf(IS)}$-ψ^*_0 and (d) $CN_{ss+sf(IS)}$-ψ_0 spaces.